



King Saud University

Arabian Journal of Chemistry

www.ksu.edu.sa  
www.sciencedirect.com



ORIGINAL ARTICLE

# Facile synthesis of eco-friendly activated carbon from leaves of sugar beet waste as a superior nonconventional adsorbent for anionic and cationic dyes from aqueous solutions



Ahmed M. Zayed <sup>a,\*</sup>, Bahaa S. Metwally <sup>a,b</sup>, M.A. Masoud <sup>a</sup>,  
Mahmoud F. Mubarak <sup>c,\*</sup>, Hussain Shendy <sup>a</sup>, Petros Petrounias <sup>d</sup>, Mahmoud S.M.  
Abdel Wahed <sup>a</sup>

<sup>a</sup> Applied Mineralogy and Water Research Lab (AMWRL), Geology Department, Faculty of Science, Beni-Suef University, Beni Suef 62521, Egypt

<sup>b</sup> Textile Technology Department, Faculty of Technology and Education, Beni-Suef University, Beni-Suef 62521, Egypt

<sup>c</sup> Petroleum Application Department, Egyptian Petroleum Research Institute, 1 Ahmed El-Zomor Street, El-Zohour Region, Nasr City, Cairo 11765, Egypt

<sup>d</sup> Chemical Process & Energy Resources Institute, Centre for Research & Technology Hellas (CERTH), Greece

Received 6 February 2023; accepted 5 April 2023

Available online 12 April 2023

## KEYWORDS

Sugar beet leaves waste;  
Thermo-chemical activation;  
Active carbon;  
Methylene blue;  
Methyl orange

**Abstract** The current study presents a unique and innovative approach to sustainable activated carbon (AC) synthesis using non-conventional agricultural wastes, leaves of sugar beet (LSB), via a thermo-chemical activation process. This approach not only offers a sustainable solution for LSB elimination, but also provides an eco-friendly alternative to commercially available activated carbon. The thermo-chemical activation process was conducted at various ratios of H<sub>3</sub>PO<sub>4</sub> / LSB (0.5:1, 1:1, 2:1, and 3:1 w/w ratios) at a fixed temperature (550 °C/2h). The unique amorphous nature, porous structure, BET surface area (S<sub>BET</sub> = 700.7 m<sup>2</sup>/g), and surface chemistry nominated the synthesized AC at 2:1 ratio as a superior adsorbent material for methyl orange, MO, and methylene blue, MB, from standard solutions in the batch system at different experimental conditions. Kinetic investigations revealed that the pseudo-second order equation explained the sorption data well. In contrast, intra-particle diffusion was not the only limiting stage in the adsorption of the addressed dyes. Similarly, the linear Langmuir equation described the adsorption data of the investigated dyes better than Freundlich one with maximum removal capacity (q<sub>max</sub>) of 185.2 and 140.8 mg/g for MB and MO, orderly. This confirms the homogenous/monolayer nature of the adsorbed ions through isoenergetic active sites upon the AC<sub>(2:1)</sub> surface. Furthermore, the electrostatic attraction was not the only leading mechanism of adsorption of both dyes, but substantial

\* Corresponding authors.

E-mail addresses: [ahmed.zayed@science.bsu.edu.eg](mailto:ahmed.zayed@science.bsu.edu.eg) (A.M. Zayed), [fathy8753@epri.sci.eg](mailto:fathy8753@epri.sci.eg) (M.F. Mubarak).

participations by hydrophobic hydrogen-bonding forces may be considered.

© 2023 Science, Technology & Innovation Funding Authority (STDF). Published by Elsevier B.V. on behalf of King Saud University. This is an open access article under the CC BY license (<http://creativecommons.org/licenses/by/4.0/>).

## 1. Introduction

AC (Activated carbon) is a type of carbonaceous material with unique characteristics such as high physicochemical stability, high porosity, mechanical strength, and a large surface area. There are numerous applications for activated carbon (Lewoyehu, 2021), including pharmaceutical (Subha and Namasivayam, 2009; Zhu et al., 2022), nuclear power stations (Kato et al., 2022), catalysis (Azargohar and Dalai, 2006; Marandi et al., 2022), separation, purification (Manoochehri et al., 2012; Natrayan et al., 2022), chemical and petroleum sectors (Ngofa et al., 2022), water treatment (Yuan et al., 2022) and others. AC is produced by oxidizing atoms found on elemental carbon's outer and inner surfaces (Al-Qodah and Shawabkah, 2009; Chatir et al., 2022; Dias et al., 2007; Guo et al., 2009; Ho et al., 2009; Idris et al., 2012; Jin et al., 2010; Sahu et al., 2010; Yahya et al., 2015). Two main distinct approaches are familiar for activated carbon production: physical and chemical preparation (Danish et al., 2011; Ekpete and Horsfall, 2011; Gayathiri et al., 2022; Hoang et al., 2022). The physical approach "dry activation," comprises two successive stages: carbonization (below 700 °C) and activation (up to 1100 °C) (Heidarnejad et al., 2020; Ketcha et al., 2012). Carbonization decreases the volatile elements of the precursor material to produce char with a more extensive fixed content of carbon. Also, the atoms of carbon undergo graphitic-like reordering during the carbonization process. The resulting charcoal is not an active product but has initial porosity and low surface area (Nazem et al., 2020). In the activation step, the carbonized charcoal reacts with oxidizing gases such as H<sub>2</sub>O (steam), air, CO<sub>2</sub> (carbon dioxide), or any mixture of these gases, therefore carbon oxides are evolved from the carbon surfaces (León et al., 2020). This is a heterogeneous and complicated process that involves the transportation of gases to the surface of the charcoal, circulation into their pores, sorption upon the pore surface, reaction with carbon, desorption, and diffusion of the prepared products into the air (Baseri et al., 2012; Sekirifa et al., 2013). But, it requires a higher activation temperature, longer activation time, and low porosity (Husien et al., 2022; Kilpimaa et al., 2015). In chemical activation "wet oxidation", the impregnation of the precursor into the selected activation agent then washing to create activated carbon, is conducted. This process needs approximately low temperatures (450 to 600 °C) and mainly relies on the capability of inorganic additives to dehydrate and degrade the cellulosic elements of the precursor (K Calderis et al., 2008; Merzougui and Addoun, 2008; Wang et al., 2022). H<sub>2</sub>SO<sub>4</sub>, K<sub>2</sub>S, KCNS (Demiral et al., 2008; Goswami and Dey, 2022), NaOH, KOH (Kielbasa et al., 2022; Zhengrong and Xiaomin, 2013) HNO<sub>3</sub>, H<sub>2</sub>O<sub>2</sub>, KMnO<sub>4</sub>, (NH<sub>4</sub>)<sub>2</sub>S<sub>2</sub>O<sub>8</sub> (Al-Qodah and Shawabkah, 2009; Guo et al., 2023; Luo et al.), K<sub>2</sub>CO<sub>3</sub> (Adinata et al., 2007; Jasri et al., 2023), ZnCl<sub>2</sub> and H<sub>3</sub>PO<sub>4</sub> (Cruz et al., 2012; Joseph et al., 2006; Karapinar, 2022) are the most commonly employed oxidizing agents (chemical catalysts). When the precursor reacts with activating agents, the oxygen groups can be added to the carbon of the precursor (Yahya et al., 2015). Depending on the employed chemical reagents, washing with acid or alkali is essentially the final step in the activation process (Md Zaini et al., 2023). This is succeeded by distilled water washing to discard the trapped chemicals in the AC porous structure (Albatrni et al., 2022). Phosphoric acid (H<sub>3</sub>PO<sub>4</sub>) has become the most popular activating agent in recent years for environmental and economic reasons (Chatir et al., 2022; El Qada et al., 2008; Ferreira et al., 2022; Neme et al., 2022). It contributes to the production of AC with enhanced mesopores and micropores (Danish et al., 2014a; Ozpinar et al.,

2022). H<sub>3</sub>PO<sub>4</sub> was predominantly utilized on lignocellulosic woody materials (Ahmad and Hameed, 2010; Budinova et al., 2006; Sirajo and Ahmad Zaini, 2023), fruits and stones (Danish et al., 2014b; Danish et al., 2022; Gratuito et al., 2008; Örkün et al., 2012; Prahas et al., 2008), and agricultural wastes (Corcho-Corral et al., 2006; Guo and Rockstraw, 2007; Ioannidou and Zabaniotou, 2007; Koyuncu et al., 2022; Li et al., 2010; Liou, 2010; Soleimani and Kaghazchi, 2007). Agricultural wastes and carbonaceous natural raw materials offer renewable, biodegradable source for activated carbon production (Karić et al., 2022). The removal efficiency of AC vary depending on the precursor materials and the activation protocol, including pyrolysis time & temperature, content of heteroatom, pore texture, surface area and charge (Tiwari et al., 2022).

Anionic methyl orange (MO) is a heavily applied water-soluble azo-dye in various industrial sectors, such as cosmetics, paper, food processing, leather, and textile (Wang et al., 2019a). The potential of MO dye to possess carcinogenic, teratogenic, and mutagenic properties is suggested (Haque et al., 2021; Sriram et al., 2022), which implies that it has the capability of causing cancer, birth defects, or genetic mutations. In addition, MO is known to be highly recalcitrant in nature, meaning it has low biodegradability and can endure in the environment for extended periods (Arumugam et al., 2022; El-Sheikh et al., 2022a; Mubarak et al., 2022). On the other hand, MB is a synthetic dye used in textile, and medical laboratory applications (Khan et al., 2022; Tuli et al., 2020), but high levels of exposure can be hazardous to human health and the environment. It can cause various adverse effects such as irreversible eye injury, vomiting, gastritis, breathing problems, nausea, cognitive confusion, painful urination, tissue death, bluish discoloration of skin, and a condition resembling methemoglobinemia. Additionally, it is considered highly carcinogenic for living beings (Bayomie et al., 2020; Liu et al., 2021; Nazir et al., 2020; Swaminathan et al., 2015; Ullah et al., 2022). Adsorption can be considered the most efficient and widely applied approach for dye remediation from aquatic environments (Aluigi et al., 2011; Ayad and El-Nasr, 2010; Gupta and Suhas, 2009; Kumar Biswal et al., 2022; Rafatullah et al., 2010; Senthil Kumar et al., 2014; Tan et al., 2008; Yao et al., 2013). This was correlated not only to its low cost but also the simplicity and easiness of operation (Kumar Biswal et al., 2022; Rafatullah et al., 2010).

Sugar beet is a strategic plant for sugar production in Egypt. The annual cultivated areas in Egypt exceed 600,000 acres. Leaves of sugar beet (LSB) represent approximately 40–50% of the harvested materials. They are made mainly of pectin (14–18%), cellulose (13–18%), and hemicellulose (11–17%), with subordinate lignin content (5–6%) and the moisture content of the dried LSB doesn't exceed 5.5%. This composition reflects their enrichment in carbohydrates, proteins, fibers, and mineral elements, such as K, Ca, Na, and Fe (Ninfali and Angelino, 2013). These greens are usually abandoned during beet root harvesting as waste causing a severe environmental problem.

The application of ACs that were produced for the first time from LSB waste, in the remediation of cationic and anionic dyes, was not investigated before. Consequently, the present study was dedicated to: 1) Recycling the widely available LSB waste in the synthesis of sustainable ACs via thermo-chemical activation procedure, and 2) Studying the effect of initial pH, contact time, adsorbent dose, and initial concentration, as the most commonly applied experimental factors, upon the remediation efficiency of cationic (methylene blue) and anionic (methyl orange) dyes by the selected AC form the prepared ones.

## 2. Materials and methods

### 2.1. Materials

The leaves of sugar beet (LSB), a common agro-residue, were collected from some sugar beet farms during harvesting season from February to June at Kom Abo Radi area, Beni-Suef Governorate, Egypt. These wastes are required to synthesize active carbon (AC). Also, 85% H<sub>3</sub>PO<sub>4</sub> was delivered from E. Merck, Germany to be applied as an activating agent for LSB during their transformation into ACs via a thermochemical activation process.

### 2.2. LSB preparation

The LSB was soaked overnight in distilled water (DW) to eliminate any adhering dust and other contaminations. After several cycles of washing, the LSB were boiled for coloration removal till getting colorless water. This was succeeded by oven drying for 24 h at 70 °C. The dried LSB sample was intensively ground by mortar and pestle below 100 µm and packed tightly for succeeding steps.

### 2.3. Active carbons (ACs) synthesis from agro-residue LSB

To activate the prepared LSB powder using an acid agent, 5 g of this powder was separately and homogeneously blended with different masses of H<sub>3</sub>PO<sub>4</sub> (2.5, 5, 10, and 15 g), to satisfy H<sub>3</sub>PO<sub>4</sub>/ LSB W/W impregnation ratios of 0.5:1, 1:1, 2:1 and 3:1, orderly. Each prepared mix was dissolved in 100 ml of DW and kept at ambient temperature overnight without any disturbance. Each permeated mixture was transferred into a programmable muffle furnace/10 °C per min for 2 h at 550 °C to complete the activation process. With distilled water and NaOH (0.1 M), the produced ACs were washed several times

thoroughly till neutralization. After, drying for 24 h at 70 °C, the AC samples were ground to < 100 µm and labeled as AC<sub>(0.5:1)</sub>, (1:1), (2:1)& (3:1) concerning the utilized acid ratio. The sketch compiling the synthesis protocol is depicted in Fig. 1.

### 2.4. Characterization of the precursor LSB and the derivative activated carbons (ACs)

The powder of the precursor LSB and the as-synthesized ACs (< 100 µm) were examined by XRD (APD-3720 diffractometer /Philips/Cu K $\alpha$  radiation/20 range of 5-80°/ scanning speed, 5° each min/ 40 kV and 20 mA), SEM (JSM-6700F/ JEOL/ Japan/energy of used beam from 20 to 30 kV/ working distance from 11.1 to 12.2 mm), FT-IR (Bruker Spectrometer/FTIR-2000/ from 400 to 4000 cm<sup>-1</sup>/ reflection resolution mode 4 cm<sup>-1</sup>) techniques to determine their crystalline phases, morphological features, and the distinctive active sites, respectively. Surface Area Analyzer (Quantachrome/ Nova 2000) was used to determine the surface area (S<sub>BET</sub>), average pore diameter (D<sub>p</sub>), and total pore volume (V<sub>t</sub>) of the materials of interest following a 2-hour vacuum degassing at 100°Celsius. Brunauer-Emmett-Teller equation was used to calculate the S<sub>BET</sub> (Brunauer et al., 1938), whereas the D<sub>p</sub> and V<sub>t</sub> were estimated by Barrett-Joyner-Halenda (BJH) one (Barrett et al., 1951).

### 2.5. Batch system experiments using aqueous solutions

Cationic (methylene blue, MB) and anionic (methyl orange, MO) dyes were selected to be remediated by the selected type of the prepared ACs in the batch system.

One gram of MO and MB was independently dissolved in one liter of distilled water, DW, to get stock solutions of 1.0 g/L. Dilutions of MO and MB stock solutions with DW were made to the appropriate concentrations for the kinetic and equilibrium experiments.



**Fig. 1** Sketch summarizing the stages of the ACs production process.

### 2.5.1. Effect of pH

To gauge the ACs<sub>(0.5:1- 3:1)</sub> removal efficiency in comparison with the precursor LSB (leaves of sugar beet) in removing the selected dyes (MO and MB) from aqueous solutions, several equilibrium experiments were conducted at various pH (2.0–10.0), maintaining the other factors constant as illustrated in **Table 1**. After centrifuging at 10000 rpm for about 15 min to separate solid from liquid (Mikro 120/Hettich/UK), the concentration of the remaining dyes in the separated liquid phases was measured by DR 6000 spectrophotometer at = 468 nm & 665 nm, for MO and MB, respectively (Mohamed et al., 2019; Subbaiah and Kim, 2016). Equations (1&2) tabulated in **Table 2** were utilized to estimate the adsorbed MO and MB amounts ( $q_e$ , mg/g) and the uptake efficiency of the applied AC (%) at equilibrium.

The results of pH experiments, to a great extend helped in deciding which type of the prepared ACs will be used for subsequent investigations.

### 2.5.2. Effect adsorbent dose

To merit the efficiency of the selected AC<sub>(2:1)</sub> in remediating the addressed dyes (MO & MB), the effect of utilized dose (10 to 35 mg), maintaining the other factors fixed as illustrated in **Table 1**. Similarly, equations 1 and 2 (**Table 2**), were employed to estimate  $q_e$  (mg/g), and the uptake efficiency (%) of the applied AC at equilibrium, respectively.

### 2.5.3. Isotherm and kinetic studies

A constant mass (20 mg) of the chosen AC<sub>(2:1)</sub> was independently introduced to 25 ml of MB and MO solutions with various initial concentrations (60 to 160 mg/L) under dynamic shaking (200 rpm)/ 2 h (**Table 1**) to configure which of the applied isotherm models will explain the data-well. The  $q_e$  (mg/g) of both MO and MB was estimated by equation 1. (**Table 2**).

The kinetic studies involved a separate addition of 25 mg of the chosen AC<sub>(1:1)</sub> to 25 ml of MO and MB with a fixed initial concentration (120 and 80 mg/L, respectively) and shaking the mixture at 200 rpm for 5, 15, 30, 60, 120, and 240 min (**Table 1**). Equations 2 and 3 cited in **Table 2**, were employed to determine the  $q_t$ , (mg/g), and R% of the applied adsorbent for the investigated dyes, orderly.

The experiments were performed at 25 ± 3 °C in triplicate, and the results have been averaged.

## 3. Results and discussion

### 3.1. Characterization of agricultural waste (LSB) and active carbons (ACs)

The XRD patterns of ACs compared to the precursor LSB were depicted in **Fig. 2**. It was revealed that the broad diffraction background in the derivative ACs which reflects the gained amorphicity after the precursor LSB, was preserved

**Table 1** The applied experimental parameters and the prevailing conditions during the conduction of the MO & MB adsorption experiments by the addressed adsorbents.

Investigated parameter	Conditions						The other parameters
pH	2	3	5	7	9	10	100 & 80 mg/L initial conc., for MO& MB, respectively, 25 mg dose, 200 rpm/ 2 h (agitation time /speed), 25 ml solution.
Adsorbent dose (mg)	10	15	20	25	30	35	pH (3.0 & 9.0), 120 & 100 mg/L of MO & MB initial conc., respectively, 200 rpm, 2 h (agitation time /speed), 25 ml solution.
Agitation time (min)	5	15	30	60	120	240	pH (3.0 & 9.0), 120 & 80 mg/L of MO & MB initial conc., respectively, 25 mg dose, 200 rpm/2h (agitation time /speed), 25 ml solution.
MO & MB initial conc., (mg/L)	60	80	100	120	140	160	pH (3.0 & 9.0) for MO & MB, respectively, 20 mg dose, 200 rpm/2h (agitation time / speed), 25 ml solution.

**Table 2** Equilibrium equations that express the MO & MB adsorption by addressed adsorbents.

Equation №	Linear form	Parameters
Eq.1	$q_e = \frac{V(C_i - C_f)}{m}$	$q_e$ (mg/g): sorbed amount of MO & MB at equilibrium $C_i$ : the initial MO & MB concentration in solutions (mg/L) $C_f$ : the concentration of MO & MB at equilibrium (mg/L) $V$ : the volume of MO & MB solutions (mL) $m$ : the mass of adsorbents (mg).
Eq.2	$q_t = \frac{V(C_i - C_t)}{m}$	$q_t$ (mg/g): sorbed amount of MO & MB at time t $C_i$ : the initial MO & MB concentration in solutions (mg/L) $C_t$ : the concentration of MO (mg/L) at time t $V$ : the volume of MO & MB solutions (mL) $m$ : the mass of adsorbents (mg)
Eq.3	$R\% = \frac{(C_i - C_f)}{C_i} \times 100$	$R\%$ : removal efficiency of MO & MB by addressed adsorbent $C_i$ : the initial MO& MB concentration in solutions (mg/L) $C_f$ : the concentration of MO & MB (mg/L) at time t

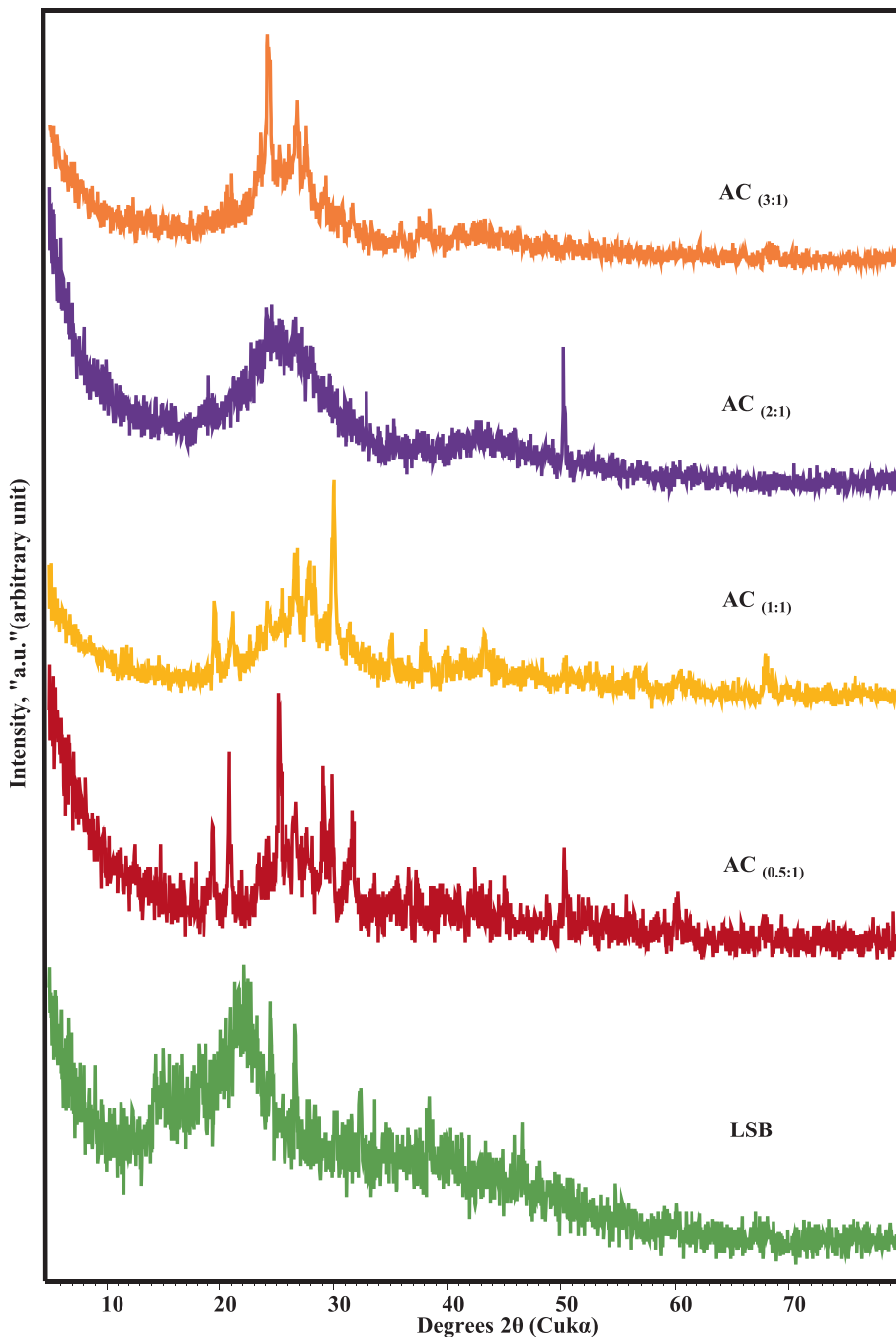


**Fig. 2** XRD patterns of the synthesized ACs in comparison with the precursor LSB.

but with less magnitude and slight shifting in  $2\theta$  values (from 20 to 30° instead of 20–25° in LSB) ([Shamsuddin et al., 2016](#)). However, some signs of improved crystallinity were traced in the derivative ACs through the emergence of some minor peaks at  $2\theta \approx 19.37$ –19.58 & 20.79–21.10°. These latter peaks could be ascribed to the  $\gamma$ -phase carbon ([Burgess-Clifford et al., 2009](#); [Mohamed et al., 2020](#)). Nevertheless, the peak intensity of this crystalline phase was reduced with the gradual rise of the utilized acid concentration till the entire absence in AC<sub>(2:1)</sub>. Furthermore, the biogenic crystalline silica in the LSB that was reflected by the moderate peak at  $2\theta = 26.7^\circ$  ([Zayed et al., 2020](#)), was masked by the approximately vital

reflection plane (002) of graphite in the derivative AC<sub>(0.5:1)</sub>, <sub>(1:1)</sub> & <sub>(3:1)</sub>, at  $2\theta \approx 26.57$ , 26.56 & 26.69°, with  $d_{(002)} \approx 3.34$ –3.36 Å, respectively. Such reflection plane (002) is approximately missing in AC<sub>(1:2)</sub> pattern as a sign of low graphitization degree. Meanwhile, the weak peaks around  $2\theta \approx 42$ –43° in AC<sub>(1:1)</sub>, <sub>(2:1)</sub> & <sub>(3:1)</sub>, might be irrelate to the graphite reflection plane (101);  $d_{(101)} \approx 2.09$ –2.14 Å. Therefore, the peaks around 26° and 43° in the prepared ACs, symbolize their amorphous nature, especially in AC<sub>(2:1)</sub> ([Xu et al., 2014](#)). This indicates the crucial role of the utilized H<sub>3</sub>PO<sub>4</sub> acid upon the graphitization degree of the ACs through the production of a more orderly arranged and densely packed microcrystalline

structure (Zhang et al., 2018). So, the applied acid not only acted as a dehydrating agent which affected the pyrolytic breakdown of LSB, but also impeded the ash development and improved carbon yield (Omri and Benzina, 2012). However, this attitude is not applicable for AC<sub>(2:1)</sub> but the amorphous nature prevails. On the level of the non-carbonaceous phase, the occurrence of a small quantity of the remaining ash after the activation process, especially at low acid concentrations, AC<sub>(0.5:1)</sub> & (1:1), was reflected by the emergence of

minor peaks of quartz at  $2\theta \approx 50.35\text{--}51.25^\circ$ ,  $60.19\text{--}60.33^\circ$  and  $68.01^\circ$ . Conversely, at the highest acid ratio (AC<sub>(3:1)</sub>), the amount of the ash remains was exceptionally minimized (Fig. 2). However, at AC<sub>(1:2)</sub>, the presence of such silicious ash was expressed at  $2\theta \approx 50.2^\circ$  as a powerful peak. The other non-carbonaceous phase is calcite that was recorded in the patterns of ACs that was formed at low acid ratios (AC<sub>(0.5:1)</sub> & (1:1)). This phase was emerged at  $2\theta \approx 29.4\text{--}29.9$  and  $30.02^\circ$ , respectively, in response of enlarged calcium occurrence of the

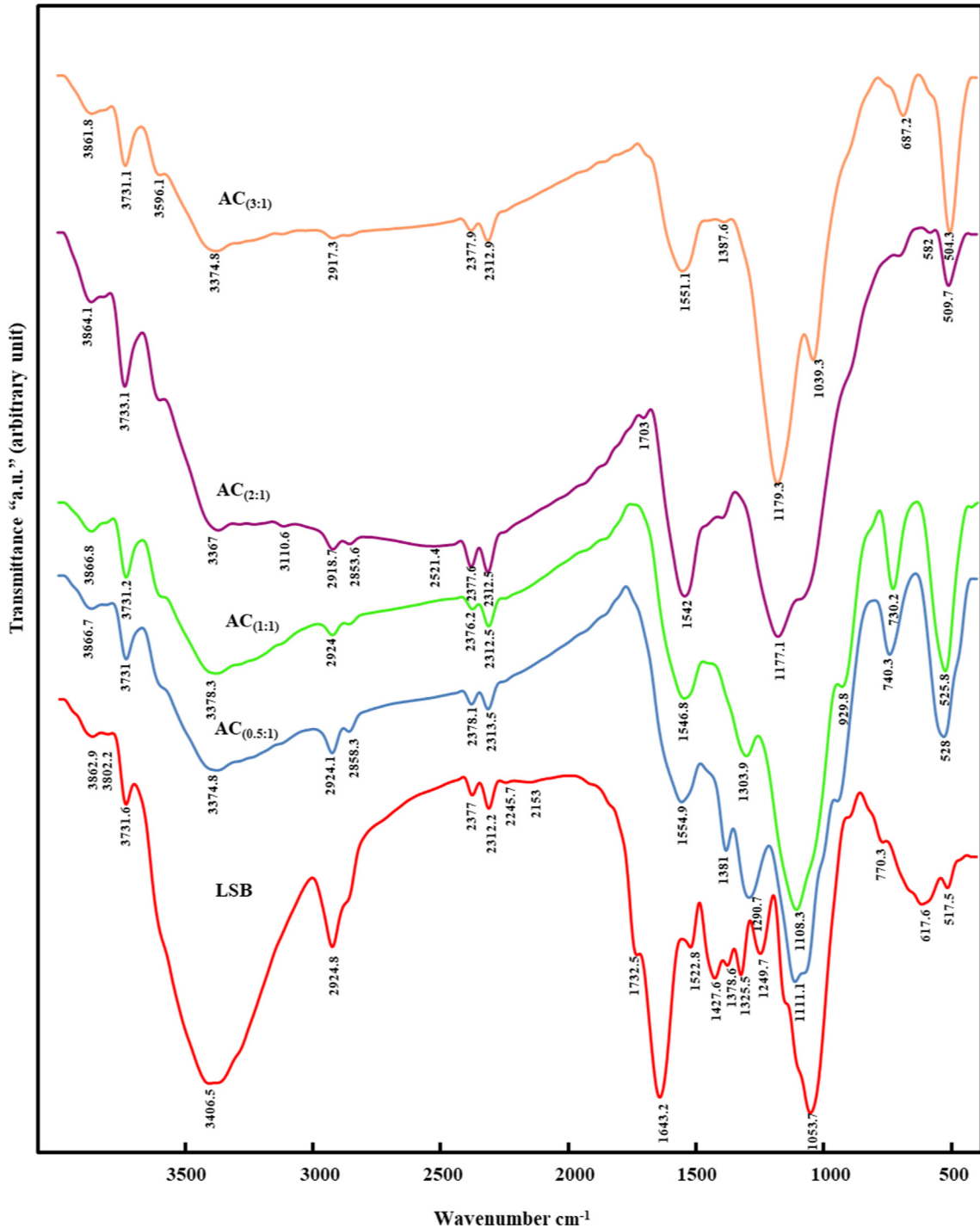


**Fig. 3** FT-IR spectra of the synthesized ACs in comparison with the precursor LSB.

precursor LSB (Fernández et al., 2017). However, the logical disappearance of this phase in AC<sub>(2:1)</sub> & (3:1), was ascribed to their approximate decomposition by the higher acid concentration during the activation process.

FT-IR spectra of the pristine LSB compared to those of their derivative ACs are given in Fig. 3. The LSB prevailing functional groups were reported at: 3406.5, 2924.8, 1634.2, and 1053.7 cm<sup>-1</sup> frequencies. The broad absorbance band at 3406.5 cm<sup>-1</sup> in the LSB spectra might be ascribed to the stretching mode of vibration of either O—H or N—H groups (Altundogan et al., 2007). In the derivative ACs, the amplitudes of N—H and/or O—H groups were gradually diminished with slight shifting to lower frequencies with increasing the applied acid concentration. In the meantime, the less intensified band at 2924.8 cm<sup>-1</sup> of the LSB that was ascribed to the stretching mode of C—H (alkenes) group of hemicellulose and cellulose (i.e., lignin polysaccharides) (Ghorbani et al., 2020; Malekbala et al., 2012), also was noticeably decreased in intensity with increasing the applied H<sub>3</sub>PO<sub>4</sub> concentration till almost complete fading in AC<sub>(1:3)</sub>. Such fading indicates the disintegration of the groups expressing the oxygenated

hydrocarbons (Shamsuddin et al., 2016). Matching with XRD outcomes, the feeble bands around 2300 cm<sup>-1</sup> of the precursor LSB, which were assigned to CO<sub>2</sub> molecules in the stretching mode (Selim et al., 2018b; Tucureanu et al., 2016), were reduced in intensity with increasing the applied acid ratio in the derivatives ACs, especially AC<sub>(3:1)</sub>. Similarly, the C=C aromatic bond (Önal et al., 2007) and/or the asymmetric stretching modes of (—COO<sup>-</sup>) group (Malekbala et al., 2012) around 1634.2 cm<sup>-1</sup> in the LSB were vanished in the spectra of the derivative ACs. Conversely, the intensity of the C=C group in the stretching mode (Anisuzzaman et al., 2015) that emerged as a shoulder band at 1522.8 cm<sup>-1</sup> in the spectra of the precursor LSB, was amplified in the derivative ACs and shifted up to higher frequencies (> 1540 cm<sup>-1</sup>) (Tucureanu et al., 2016). This reflects a remarkable improvement in the aromatic characteristics of prepared ACs via the aliphatic component's transformation in the pristine LSB (Kumar and Jena, 2016). The 1053.7 cm<sup>-1</sup> intensified band in the LSB may be correlated with C—O stretching (Malekbala et al., 2012). With increasing the applied acid ratio, the C—O group (1053.7 cm<sup>-1</sup>) was shifted up to higher frequencies in the

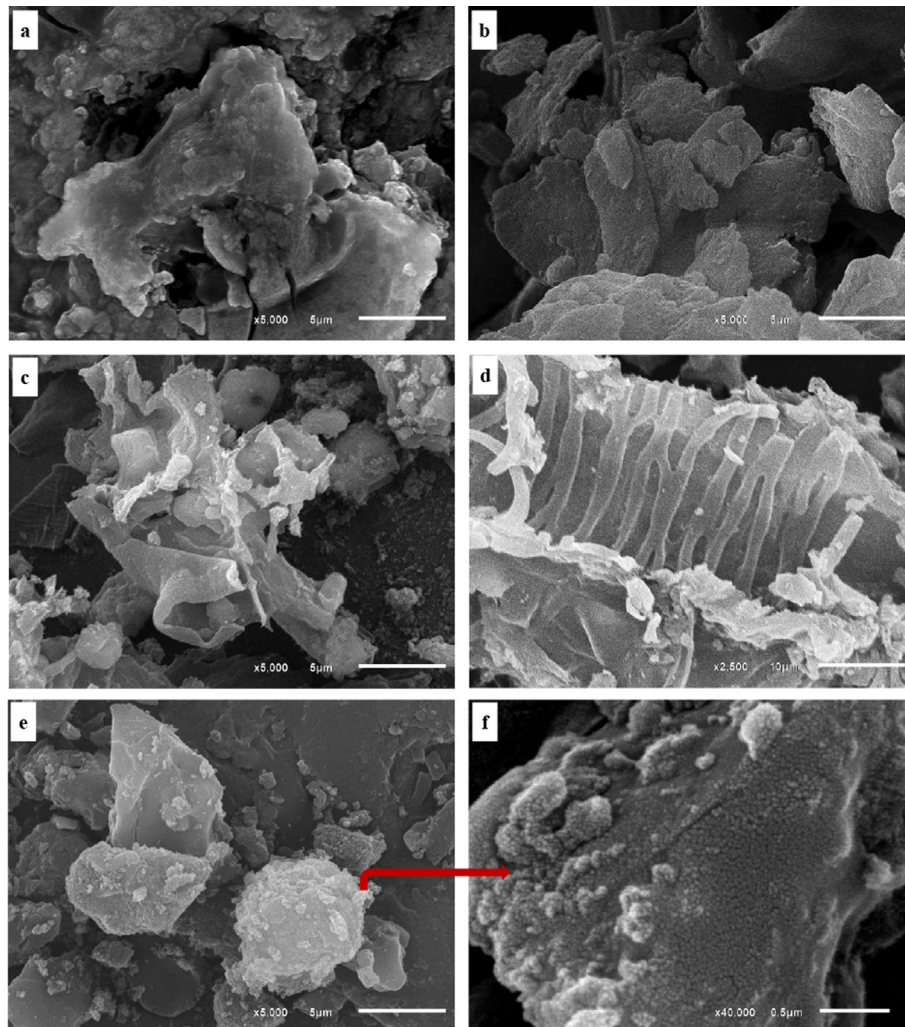


**Fig. 4** SEM images with different magnifications showing: (a-b) LSB with nodular crenulation as a reflection of rough surface; (c) AC (0.5:1) with rough surface and agglomerated spherical-like nanoparticles; (d) Survived texture of the LSB after acid activation to prepare AC (0.5:1) as a sign of in-complete activation; (e-f) Spherical-like nanoparticles of AC (1:1).

derivative ACs ( $\approx$ 1111-1179 cm $^{-1}$ ), indicating the coupling between the stretching mode of O—C group within the aromatic P—O—C linkages and hydrogen-bonded P=OOH groups from polyphosphates/and or phosphates (Han et al., 2020; Xu et al., 2014). Also the emergence of stretching vibration mode of P=O group in AC<sub>(0.5:1)</sub> and AC<sub>(1:1)</sub> at 740.3 and 730.2 cm $^{-1}$ , respectively, can be correlated to the applied H<sub>3</sub>PO<sub>4</sub> (Anisuzzaman et al., 2015). Moreover, the remarkable occurrence of the band at 687.2 cm $^{-1}$  only in AC<sub>(3:1)</sub> and the bands at 528, 525.8, 509.7 and 504.3 cm $^{-1}$ , in all derivative ACs confirms the existence of out of plane deformation for the C—H that belong to benzene and alkenes derivatives with various grade of substitution (Canales-Flores and Prieto-García, 2020; Suganya and Senthil Kumar, 2018).

The SEM investigations displayed that both the precursor LSB and the derivatives ACs have rough and heterogeneous surfaces crowded with nodular crenulation as a reflection of rough surface, with the preference of the derivatives (Fig. 4a-f & Fig. 5a-d). The porous nature of the surfaces in the as-synthesized ACs can be tied to the H<sub>3</sub>PO<sub>4</sub> evaporation during the carbonization process (Han et al., 2020; Kumar and Jena, 2016).

Concerning AC<sub>(0.5:1)</sub>, the applied low acid concentration, resulted in immature activation process that contributed to the preservation of some survived texture of the precursor LSB (i.e. as a sign of incomplete activation process) side by side with a rough surface and agglomerated spherical-like nanoparticle as a reflection of a more surface heterogeneity

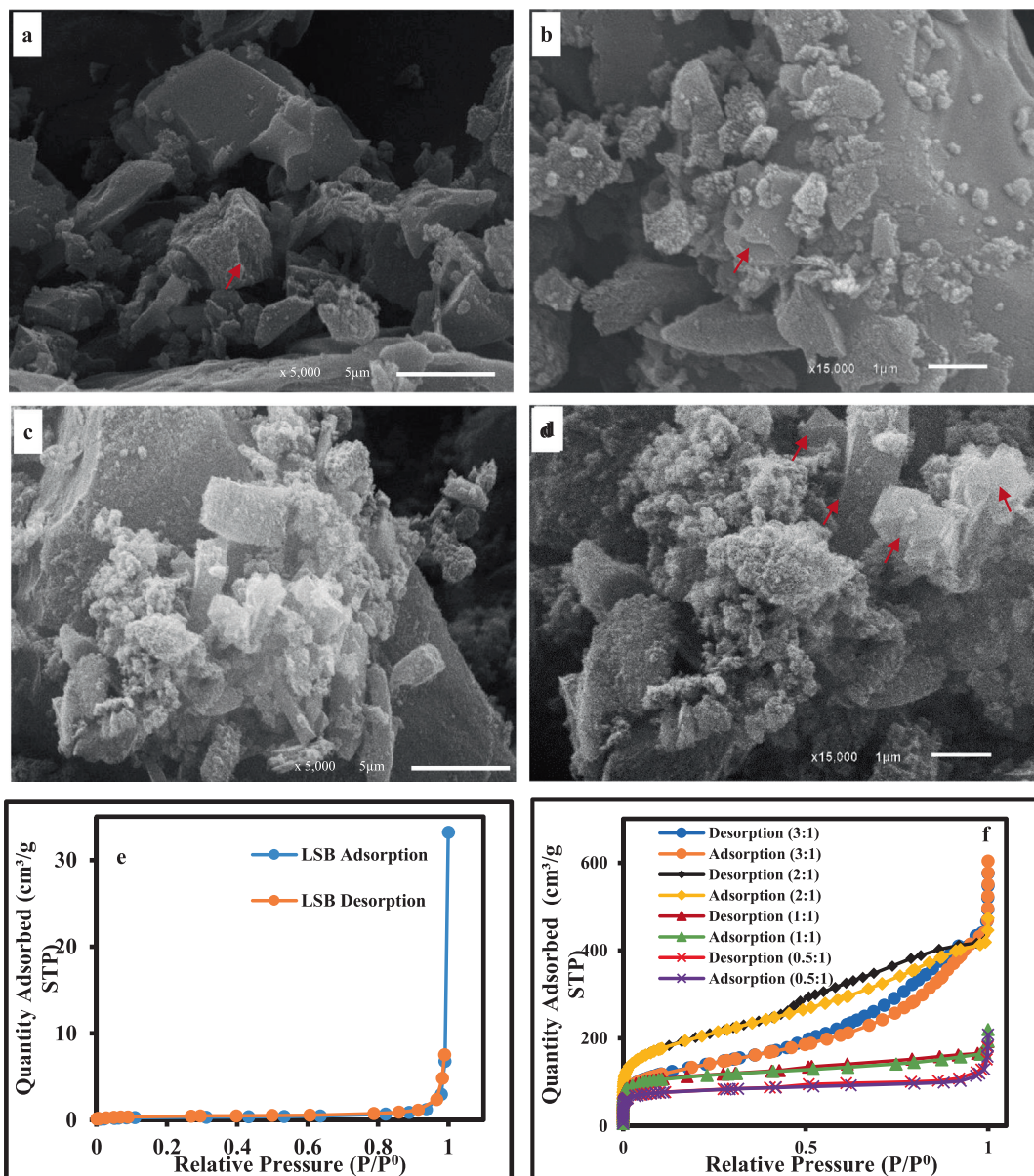


**Fig. 5** SEM images with different magnifications showing: (a,b) Spherical-like nanoparticles of AC (2:1) as a reflection of high amorphicity as well as grooves and cavities produced by the activating agent during the activation process of AC(2:1); (c-d) High graphitization degree with ideal prismatic crystals in AC(3:1) as a reflection of high crystallinity side by side with spherical-like nanoparticles indicating the remaining traces of the amorphous nature; (e) Nitrogen adsorption–desorption isotherms of LSB; (f) Nitrogen adsorption–desorption isotherms of the prepared ACs.

(Fig. 4c&d). Beyond 0.5:1 acid ratio (i.e., in AC<sub>(1:1 & 2:1)</sub>), the primary texture of the LSB was entirely destroyed as a sign of a mature carbonization process (Fig. 4e-f & Fig. 5a-b). Therefore, the amount of the produced spherical nanoparticles upon the surfaces of these ACs was amplified. Some cavities and grooves were also created upon the precursor LSB surface by the activating agent during the activation process of AC (2:1) (Fig. 5b). Furthermore, the intensified occurrence of these nanoparticles upon their surfaces reflects the amorphicity degree of the prepared ACs, especially AC<sub>(2:1)</sub> in agreement with XRD data. However, the application of higher acid concentration (i.e. 3:1 ratio) improved the graphitization process of the organic carbon of the LSB to the limit that graphite crystals with the ideal prismatic habit (hexagonal shapes) were produced as a reflection of a high degree of crystallinity in AC<sub>(3:1)</sub> (Fig. 5c-d), matching with XRD data. Meanwhile, the occurrence of spherical-like nanoparticles in juxtaposition with the prismatic graphite crystals signifies that amorphous nature traces are still preserved in AC<sub>(3:1)</sub>.

The N<sub>2</sub> isotherms of LSB and their derivative ACs are illustrated in Fig. 5e-f. The precursor LSB displayed type III isotherm following the IUPAC classification (Thommes et al., 2015). This denotes that the investigated LSB has a macroporous habit with poorly connected semi-closed pore as was assured by the overlapping of the two branches of the given isotherm (Fig. 5e). The partial pore disconnection resulted in geometrical parameters with low quality ( $S_{BET} = 1.5 \text{ m}^2/\text{g}$ ,  $V_t = 0.0107 \text{ cm}^3/\text{g}$  and  $D_p = 28.7 \text{ nm}$ ).

On the contrary, the displayed isotherms of the derivative ACs were hybrid depending on the applied concentration of H<sub>3</sub>PO<sub>4</sub> acid (Fig. 5f). These various isotherms (from type II to IV) with respect to IUPAC classification (Kumar and Jena, 2016), denote microporous/mesoporous/macroporous characteristics of the produced ACs. These isotherms followed Type II in behavior with noticeable N<sub>2</sub> adsorption via the accessible micropores at the applied low relative pressure (P/P<sup>0</sup>) (Kumar and Jena, 2016). Conversely, these isotherms went along with type IV that displayed hysteresis loops of type H<sub>4</sub> at the applied P/P<sup>0</sup> of medium and high intensities, signifying monolayer/multilayer N<sub>2</sub> adsorption (Kumar and Jena, 2016). Furthermore, raising the acid concentration ratio from 0.5:1 to 2:1, was coupled with development in N<sub>2</sub> adsorption, signaling the gradual porosity improvement in the produced AC. In contrast, beyond 2:1 (i.e., 3:1), a noticeable decline in N<sub>2</sub> adsorption was recorded in line with the wall demolition among the neighboring pores. Therefore, the total porosity

and surface area of such active carbon were minimized (Sych et al., 2012).

Additionally, the progressive broadening of the hysteresis loops with increasing the applied acid assures these mesopores domination in the prepared AC. Likewise, the debility to attain the state of equilibrium of N<sub>2</sub> uptake by ACs, indicates the wide range of pore diameters.

The results of the geometrical parameters of the derivative ACs are compiled and compared with those of the precursor LSB (Table 3). It was displayed that the gradual increase in the utilized acid ratio from 0.5:1 to 3:1, resulted in a remarkable development in  $V_t$  (0.01 to 0.68 cm<sup>3</sup>/g, orderly), indicating an important role of the activating agent in enhancing the ACs porosity via lignin structure destruction and the minimization of LSB cellulose (Tuli et al., 2020). For D<sub>p</sub>, the low H<sub>3</sub>PO<sub>4</sub> ratios (0.5:1 and 1:1) had an approximately equivalent impact;  $D_p \approx 2.5 \text{ nm}$ . Nevertheless, further increase in acid ratios (2:1 and 3:1), contributed to a noticeable raise in the D<sub>p</sub> (3.7 and 5.7 nm, respectively).

Additionally, the S<sub>BET</sub> of all investigated ACs displayed a progressive enhancement from AC<sub>(0.5:1)</sub> to AC<sub>(2:1)</sub> (Table 3). Conversely, the S<sub>BET</sub> of the AC<sub>(3:1)</sub> declined to  $\approx 480 \text{ m}^2/\text{g}$  although the high applied acid ratio. This S<sub>BET</sub> reduction can be tied with the improved crystallinity through an evolving of idioblastic hexagonal crystals of graphite in the AC<sub>(3:1)</sub> compared with the other ACs, matching with XRD and SEM outcomes.

### 3.2. Batch system experiments using aqueous solutions

#### 3.2.1. Effect of pH

The MO remediation by the prepared ACs<sub>(0.5-1-3:1)</sub> and their precursor LSB is a pH-dependent process. Unlike the precursor LSB, ACs<sub>(1:1-3:1)</sub> displayed very high MO removal efficiency (R% > 97%) at pH 2.0–3.0 (Fig. 6a); the maximum R% was reached at pH 3.0 (> 99%), in an agreement with preceding investigations (El-Sheikh et al., 2022b; Subbaiah and Kim, 2016; Zayed et al., 2018). On the contrary, AC<sub>(0.5:1)</sub> displayed a slightly high MO removal efficiency (R% > 92%) in both pH values (pH 2.0–3.0) in favor of the more acidic one. The exceptional sorption efficiency of the ACs for MO over LSB, was correlated with their higher geometrical parameters as was discussed before in the first technical report. Far of pH 5.0, MO sorption was slightly diminished, particularly in the basic medium, matching with the outcomes of pH<sub>PZC</sub> (point of zero charge) that was estimated following Singh

**Table 3** Geometrical parameters of the LSB compared to the derivative ACs obtained from the nitrogen adsorption/desorption isotherms.

Sample	Surface area (m <sup>2</sup> / g)			Pore volume (cm <sup>3</sup> / g)			Average pore diameter (nm)
	BET (S <sub>BET</sub> )	Mesopores (S <sub>Meso</sub> )	Micropores (S <sub>Micro</sub> )	Total pore volume (V <sub>t</sub> )	Meso-pore volume (V <sub>Meso</sub> )	Micro-pore volume (V <sub>Micro</sub> )	
LSB	1.50	0.54	0.96	0.01	0.004	0.006	28.70
0.5:1	300.30	120.1	180.2	0.20	0.08	0.12	2.68
1:1	416.80	126.4	290.4	0.26	0.08	0.18	2.48
2:1	700.70	440.2	260.5	0.65	0.41	0.24	3.69
3:1	480.60	356.2	124.4	0.68	0.50	0.18	5.70

et al. protocol (Singh et al., 2015). Such outcomes demonstrated that the ACs ( $_{(0.5:1-2:1)}$ ) and its LSB surfaces are consistently negative except between  $\approx$  pH 3.1 to 6.8 at which their surface has positive charges ( $pH_{PZC}$  of LSB  $\approx$  2.9 and 6.75,  $AC_{(0.5:1)} \approx$  3.1 and 6.9,  $AC_{(1:1)} \approx$  3.1 and 6.9,  $AC_{(2:1)} \approx$  3.2 and 6.7) (Fig. 6b). On the contrary,  $AC_{(3:1)}$ , revealed negative charge along the investigated pH interval. Specifically, the electrostatic interactions between the binding sites of the studied sorbents and the negative sulfonate group ( $-SO_3^-$ ) of MO ions in solution were facilitated by the higher degree of ionization of MO ( $pK_a = 3.46$ ; (Asuha et al., 2010; Umpuch and Sakaew, 2013)) and the protonation of the ACs and LSB surfaces at pH 3.0. In this situation, hydrogen ions function as bridging ligands between the MO anions and the targeted adsorbent surfaces during the protonation process. On the contrary, the presence of competitive  $OH^-$  ions in the solution caused deprotonation of sorbent's surfaces, generating repulsive interactions against MO anions and reducing its uptake

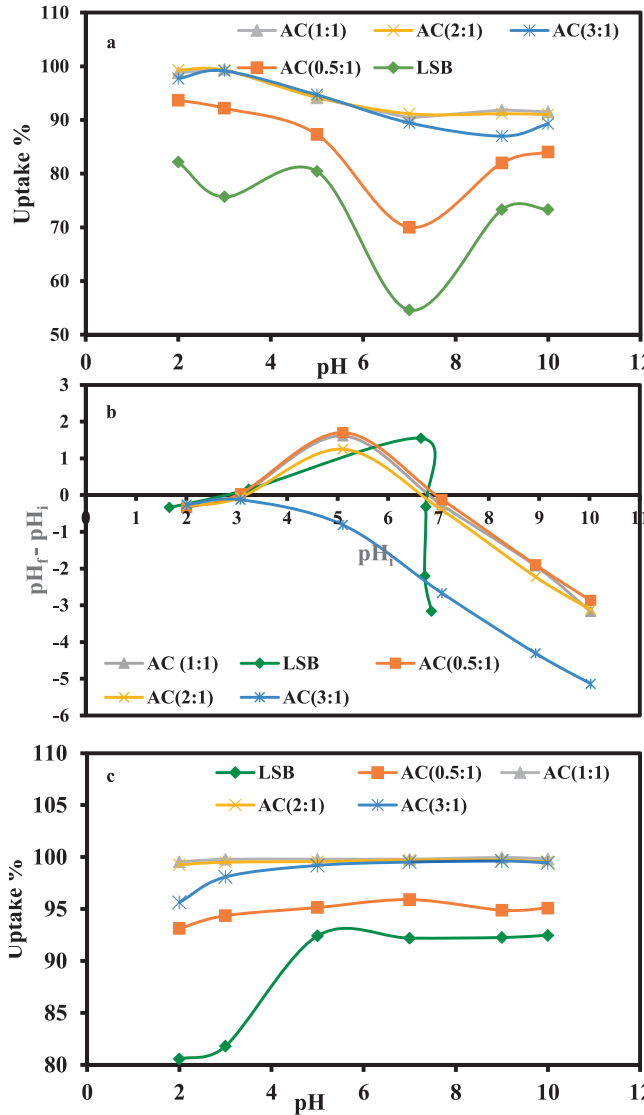


**Fig. 6** Plots of  $AC_{(0.5:1-3:1)}$  compared to their precursor LSB showing: (a) Effect of pH on MO uptake; (b) Zero charge points; (c) Effect of pH on MB uptake.

(Mohammadi et al., 2011). As a result, pH 3.0 was chosen as the experimental pH for the following experimental work.

Although electrostatic contact is a major factor, additional hydrophobic forces (hydrogen bonding, H-bonding) may also play a significant role in the sorption of MO by the targeted adsorbents (Tran et al., 2017a; Zayed et al., 2020). The hydrophobicity of graphite and/or organic matter contents of ACs and LSBs is likely to be the source of these forces (Akhair et al., 2018; Yee et al., 2009). Two types of hydrogen bonding interactions have been identified: 1) dipole–dipole and 2) Yoshida (Tran et al., 2017a; Zayed et al., 2020). The interaction among surface hydroxyl groups of the investigated sorbents and the aromatic rings of the MO, denotes the 2nd sort of H-bonding (Tran et al., 2017a; Zayed et al., 2020). Whereas the interaction that connects the MO's nitrogen /oxygen atoms

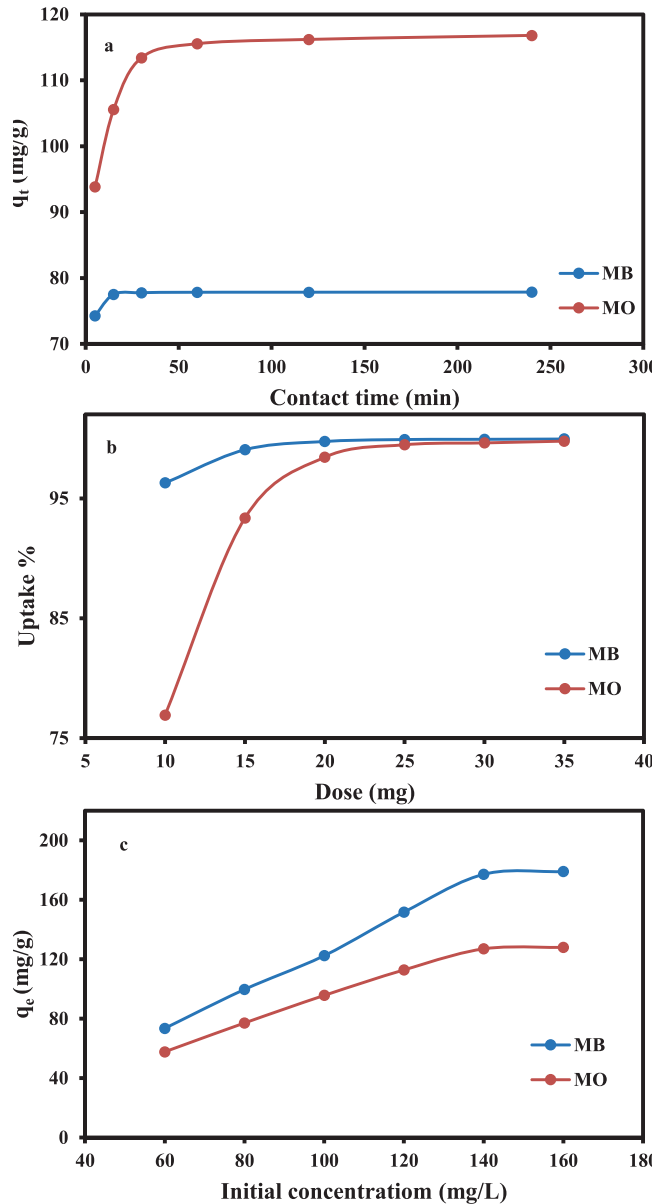


**Fig. 7** Plots showing: (a) Effect of contact time; (b) Effect of dose; (c) Effect of initial concentration on MO & MB uptake by the applied  $AC_{(2:1)}$ .

(H-acceptor) to the accessible hydrogen atoms (H-donor) of the sorbent's hydroxyl groups, signifies the 1st sort of H-bonding (Tran et al., 2017a; Zayed et al., 2020). The significant sorption efficiency of MO by the targeted adsorbents at pH 9.0–10.0 (73.3 to 91.9%), despite the presence of  $\text{OH}^-$  as competing ions in the solution, confirmed the participation of H-bonding process.

Similarly, the initial pH played a critical role in MB uptake by the addressed adsorbents from the aqueous solution (Fig. 6c). Unlike the parental LSB, the prepared ACs revealed high removal capacity ( $R\% = 93$  to 99.96%) in pH range from 3.0 to 10.0; equilibrium was reached at pH 9.0 ( $R\% > 99$ ) for all the investigated ACs (1:1-3:1), except for  $\text{AC}_{(0.5:1)}$  that displayed only  $R\% = 94.8\%$ . Far away from pH 9.0, MB removal by the addressed adsorbents presented no considerable increase in the R%.

The high MB uptake efficiency at pH 2.0, 3.0, and 5.0 ( $> 93\%$ ) despite the intense competition with  $\text{H}^+$  ions, implies that electrostatic forces (i.e non-hydrophobic forces) cannot be counted as the main mechanism for MB remediation by the regraded sorbents; other forces can be counted as a driving force for MB adsorption (Tran et al., 2017b).

The high MB uptake capacity by the regarded adsorbents at basic mediums, nominated pH 9.0 for executing the following experimental work.

Based on the previously discussed geometrical parameters and the pH experiments' results,  $\text{AC}_{(2:1)}$  was selected for remediation of both MB and MO in the succeeding experimental parameters.

### 3.2.2. Effect of contact time

Studies conducted at various equilibrium times demonstrated that the adsorption of MO ions by  $\text{AC}_{(2:1)}$  was very fast in the time interval from 5 to 30 min, with  $q_t$  ranging from 93.83 to 113.42 mg/g, respectively (Fig. 7a). This can be correlated with the high surface area of the regarded sorbent with plentiful available binding sites (Saleh et al., 2014). However, equilibrium was attained at 60 min, expressing the chemical character of the adsorption process of MO ions by the regarded sorbent (Cheah et al., 2013; Chen et al., 2010). After 60 min, no appreciable  $q_t$  was achieved (115.54–116.8 mg/g).

Similarly, MB uptake (Fig. 7a) by  $\text{AC}_{(2:1)}$  was very speedy during retention times between 5 and 15 min (74.28 and 77.51 mg/g, respectively) indicating that the adsorption process is a time-controlled one (Kim et al., 2016). This was linked to the abundance of free binding sites on the AC surface, which

**Table 4** Adsorption kinetics and isotherm models for MO & MB uptake by  $\text{AC}_{(2:1)}$  adsorbent.

Kinetic/ isotherm Model	Linear form	Parameters	Refs.
Pseudo- second-order	$\frac{t}{q_t} = \frac{1}{k_2 - q_e^2} + \frac{t}{q_e}$	$q_t$ (mg/g): removed amount of MO & MB at time t. $q_e$ (mg/g): equilibrium adsorption uptake. $k_2$ (g/mg min): rate constant of the second-order adsorption. $q_e^{(calc.)} = 1/\text{slope}$ $k_2 = (\text{slope})^2/\text{intercept}$	(Ho and McKay, 1999)
Intra-particle diffusion	$q_t = k_p t^{1/2} + C$	$q_t$ (mg/g): removed amount of MO & MB at time t. $K_p$ (mg/g min <sup>0.5</sup> ): intra-particle diffusion rate constant. $C$ (mg/g): intercept of the line which reflects the thickness of the boundary layer. $k_p = \text{slope}$ $C = \text{intercept}$	(Weber and Morris, 1962)
Langmuir	$\frac{C_e}{q_e} = \frac{1}{q_{\max} K_L} + \frac{C_e}{q_{\max}}$	$C_e$ (mg/L): equilibrium concentration of the resting MO & MB in the solution $q_e$ (mg/g): removed amount of MO & MB at equilibrium. $q_{\max}$ (mg/g): maximum adsorption capacity $K_L$ (L/mg): Langmuir constant $q_{\max} = 1/\text{slope}$ $K_L = \text{slope}/\text{intercept}$	(Langmuir, 1916)
$R_L = 1/(1 + K_L C_0)$ $R_L > 1$ (unfavorable adsorption) $R_L = 1$ (linear adsorption) $(0 < RL < 1)$ (favorable adsorption) $R_L = 0$ (irreversible adsorption)		$R_L$ : Equilibrium parameter of Langmuir equation. $C_0$ : Initial MB & MO concentration.	(Weber and Chakravo, 1974)
Freundlich	$\log q_e = \log K_F + \frac{1}{n} \log C_e$	$C_e$ (mg/L): equilibrium concentration of the resting MO & MB in the solution $q_e$ (mg/g): removed amount of MO & MB at equilibrium. $K_F$ (mg/g) <sup>1/n</sup> L/mg: MO & MB adsorption capacity. $n$ : heterogeneity factor. $k_F = 10^{\text{intercept}}$ $1/n = \text{slope}$	(Freundlich, 1906)

were available to interact with MB ions (Agarwal et al., 2016). After 15 min, there was no discernible increase in the MB adsorption rate ( $q_t$  77.8 mg/g), indicating that equilibrium had been reached. Rapid equilibrium suggests the chemical basis of MB adsorption and nominates AC<sub>(2:1)</sub> as a suitable adsorbent for MB absorption.

### 3.2.3. Effect of adsorbent dose

Removing MO from a solution with an initial concentration of 120 mg/L using variable masses (10 to 35 mg) of AC<sub>(2:1)</sub> was analyzed deeply (Fig. 7b). By raising the mass of the regarded AC from 10 mg to 20 mg, the MO elimination capacity rose from 76.9% to 98.5%. However, the MO absorption capacity increased only marginally (99.8%) when a mass of > 20 mg was used. This logical progression leading to equilibrium can be irrelated to the number of binding sites (O- and N-containing groups) on the AC's surface (Mokhtari et al., 2016; Saleh et al., 2014).

As well, the R% of MB at various masses of the addressed AC (10 to 35 mg) displayed that equilibrium state (R% > 99%) was attained by increasing the applied dose beyond 10 mg (Fig. 7b). This can be justified by the occurrence of bountiful unoccupied active sites upon the AC surface (Mokhtari et al., 2016; Saleh et al., 2014).

So the optimum masses of AC<sub>(2:1)</sub> application in the adsorption of MB and MO was 15 and 20 mg, respectively.

### 3.2.4. Effect of initial concentration

The progressive raise in the initial concentration of applied MO (60–160 mg/L) was accompanied by an improvement in  $q_e$  (mg/g) from 57.7 to 128.02 mg/g (Fig. 7c). This can be accounted by the developing rate at which MO ions collide with the AC's sites. In addition, the elevated mass gradient that propelled the MO ions to the AC surface was the source of the sorption improvement (Shiue et al., 2012).

Likewise, the development of MB concentration from 60 to 160 mg/L, enhanced the attained  $q_e$  (mg/g) per unit mass of the regarded AC<sub>(2:1)</sub> till equilibrium (Fig. 7c).

### 3.2.5. Isotherm studies

The linear form of two of the widely used isotherm models (Langmuir and Freundlich models) was employed to elucidate the interactive nature between the adsorbate (MO & MB) and AC<sub>(2:1)</sub> (Freundlich, 1906; Langmuir, 1916) and to get helpful information about the surface properties of the regarded sorbent and their affinity to the probed dyes. Tables 4 and 5 display these linear equations and their estimated parameters, respectively. Therefore, the plots of  $C_e/q_e$  vs.  $C_e$  and  $\log q_e$

vs.  $\log C_e$ , were employed to estimate the Langmuir and Freundlich parameters, orderly (Fig. 8).

The Langmuir isotherm presupposes that the adsorption process occurs at discrete isoenergetic binding sites on the sorbent surface in form of a monolayer (Chen et al., 2010; Hameed, 2009). Oppositely, the Freundlich isotherm assumes the adsorbate will be compiled as several layers (a heterogeneous adsorption process) on the sorbent surface (Selim et al., 2018a).

Adsorption data of the probed dyes by AC were best characterized by Langmuir isotherm, as was evident from the determination coefficient results of the two applied models (i.e.,  $R^2 = 0.9997$  and 0.9992 for MO and MB, respectively, using Langmuir equation) (Table 5). As a result, the adsorbed MO and MB ions formed monolayers on the negatively and positively charged isoenergetic sites upon the AC surface

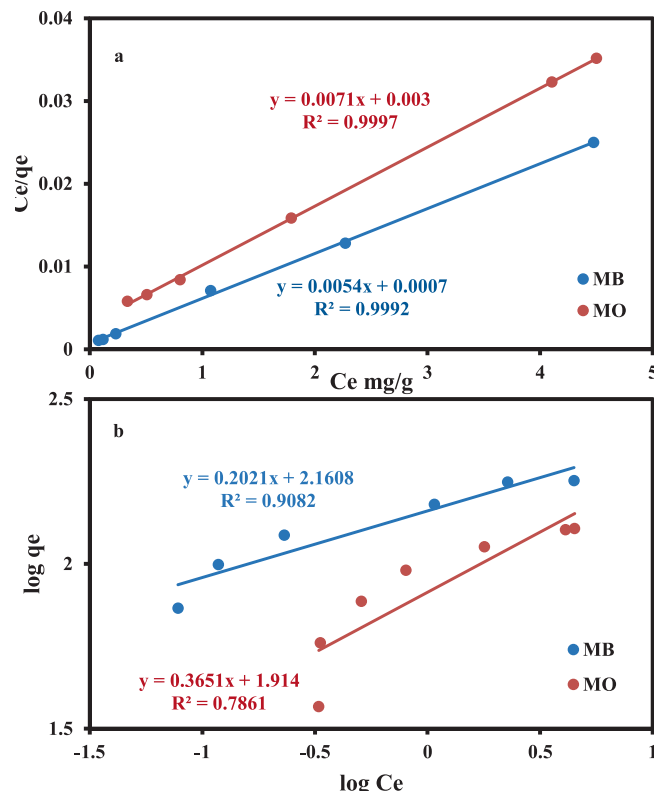


**Fig. 8** Isotherm linear plots for MB and MO removal by AC<sub>(2:1)</sub> using: (a) Langmuir; (b) Freundlich equations.

**Table 5** The isotherm parameters of the MO & MB adsorption by AC<sub>(2:1)</sub> adsorbent.

Initial concentration (60–140 mg/L)	Isotherm Model					
	Langmuir			Freundlich		
	Parameters			Parameters		
	$q_{\max}$ (mg/g)	$K_L$ (L/mg)	$R^2$	$1/n$	$K_F$ (mg/g) $^{1/n}$	$R^2$
MB	185.2	7.714	0.9992	0.2021	144.8105	0.9082
MO	140.8	2.367	0.9997	0.3651	82.035	0.7861

(Chen et al., 2010; Jawad et al., 2019b; Jawad et al., 2019c). The Langmuir equilibrium parameter  $R_L$  for both dyes, was also determined using the formula presented in Table 5. The values of  $R_L$  for MB and MO ranged from 0.0008 to 0.0022 and 0.003 to 0.011, orderly (positive,  $0 < R_L < 1$ ). These obtained values indicate that Langmuir could be utilized to adequately present the adsorption data for both dyes via AC<sub>(2:1)</sub>.

However, the discrepancy in  $q_{\max}$  (the maximum adsorption capacity) of MO and MB ions (140.80 and 185.20 mg/g, orderly) endorses the larger played role of the negative active site than the positive ones (Cunha et al., 2020) and hence the more considerable affinity for MB compared to MO (i.e., the overall number of acidic sites is larger than the basic ones matching with other previous studies). So, the prepared AC<sub>(2:1)</sub> can be classified as an effective sorbent for such dye species.

A comparison of the  $q_{\max}$  of MO and MB remediation by the addressed AC<sub>(2:1)</sub> with other adsorbents showed the superiority of the current adsorbent over the other investigated natural, modified, and synthetic ones (Table 6).

### 3.2.6. Kinetic studies

The linear expression of the PSO “pseudo-2nd-order” and IPD “inter-particle diffusion” equations were employed to elucidate the kinetics of MB & MO sorption by AC sorbent (Ho and McKay, 1999) (Table 4). Also, the parameters of these models were estimated and tabulated in Table 7.

The MO and MB sorption process by the AC<sub>(2:1)</sub> was illustrated-well by PSO equation (Fig. 9a). This implies that chemisorption could be the rate-governing step of their removal (Hasanzadeh et al., 2020; Jawad et al., 2019a; Norouzi et al., 2018) as was assured by the obtained  $R^2$  (one for both dyes) (Mohamed et al., 2019; Wang et al., 2011). As well, this was confirmed through the close matching between the calculated ( $q_e^{(cal)} = 78.125$  and 117.65 mg/g, for MB and MO, orderly) and the experimental  $q_e$  ( $q_e^{(exp.)} = 77.51$  and 115.54 mg/g, for MB and MO, orderly) (Table 7).

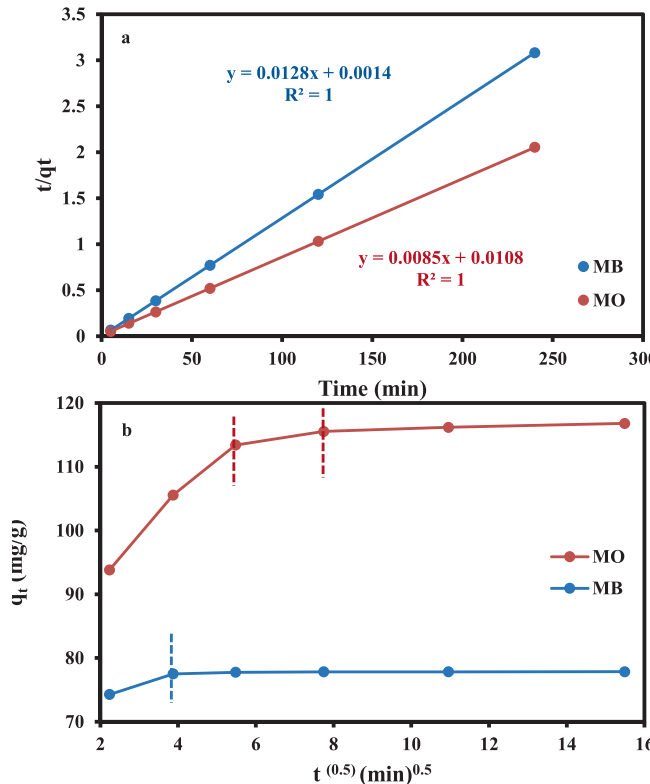
Furthermore, the IPD equation that was graphically displayed through  $q_t$  vs.  $t^{0.5}$  plotting, gave a multistage linear plot deviating away from the origin; 2 and 3 stages for MB and MO, were recorded (Fig. 9b). These multilinear plots denote that MB and MO sorption by the AC was not mainly illus-

**Table 6** Adsorption capacity for MO and MB by some natural, modified and synthetic materials in comparison with the AC<sub>(2:1)</sub> of the present study:  $q_{\max}$  obtained from the Langmuir constant.

Adsorbent	Adsorption capacity $q_{\max}$ (mg/g) of MO	Adsorption capacity $q_{\max}$ (mg/g) of MB	Reference
Cellulose/clay composite hydrogel	—	277	(Wang et al. 2019b)
Zeolite/chitosan composite	—	199	(Khanday et al. 2017)
Sericin/β-cyclodextrin/PVA composite	—	261	(Zhao et al. 2015)
Halloysite-Cyclodextrin Nanosponges	—	226	(Massaro et al. 2017)
Chitosan/polyvinyl alcohol/zeolite	153	—	(Habiba et al. 2018)
Cotton fiber	—	113	(Xiong et al. 2014)
Modified pine sawdust. sawdust	—	84	(Zhang et al. 2015)
Fe-MIL-88NH2	—	15.99	(Fu et al. 2021)
ZIF-8@SiO2@MnFe2O4	78.12	—	(Abdi et al. 2019)
Fe-MIL-88NH2	58.72	—	(Fu et al. 2021)
Poly(N-isopropyl acrylamide-coitaconic acid)/crosslinked with OVPOSS	—	130	(Eftekhari-Sis et al. 2018)
Carboxymethyl cellulose coated Fe3O4@SiO2 magnetic nanoparticles	—	17.5	(Zirak et al. 2018)
β-CD-SNHS	—	99.22	(Ebadi and Rafati 2015)
Co3O4 nanocube-doped polyaniline	107	—	(Shahabuddin et al. 2016)
Modified PAN	99.15	—	(Chauque et al. 2017)
Activated clay	16.78	—	(Ma et al., 2012)
Maghemite/chitosan nano-composite films	29.41	—	(Jiang et al., 2012)
Bentonite	33.8	—	(Leodopoulos et al., 2012)
Organic matter rich clays (OMRC)	41.67	—	Zayed et al., 2018
Calcinated organic matter rich clays (COMRC)	34.48	—	Zayed et al., 2018
Modified wheat straw	50.4	—	(Su et al., 2014)
Modified coffee waste	62.5	—	(Lafi and Hafiane, 2016)
Mesoporous carbon CMK-3	294.1	—	Mohammadi et al., 2011
Powdered activated carbon modified by HNO <sub>3</sub>	384.62	—	(Do et al., 2011)
Activated carbon/Fe <sub>3</sub> O <sub>4</sub> nanoparticle composites (10Fe <sub>3</sub> O <sub>4</sub> /PAC-HNO <sub>3</sub> )	303.03	—	(Do et al., 2011)
Ephedra strobilacea char (ESC)	—	31.055	Agarwal et al.(2016)
Phosphoric acid modified Ephedra strobilacea char (ESP)	—	21.88	Agarwal et al.(2016)
Zinc chloride modified Ephedra strobilacea char (ESZ)	—	37.174	Agarwal et al.(2016)
Alginate/almond peanut biocomposite	—	22.8	Erfani and Javanbakht (2018)
AC <sub>(2:1)</sub>	140.8	185.2	Current study

**Table 7** The kinetic parameters of the MO & MB adsorption by AC adsorbent.

Adsorbent	Dye	Initial concentration (mg/L)	$q_e^{(exp.)}$ (mg/g)	Kinetic Model
<b>AC (2:1)</b>				Pseudo-second order
	MB	80	77.51	$k_2$ (g/mg min) $q_e^{(Calc.)}$ (mg/g) $R^2$
	MO	120	115.54	0.1117    78.125    1 0.0067    117.65    1

**Fig. 9** Linear plots for MB and MO remediation by  $AC_{(2:1)}$  using: (a) Pseudo-second order; (b) Intra-particle diffusion equations.

trated by IDP but several types of diffusion may be intervening (Abdulhameed et al., 2019; Gusain et al., 2016; Selim et al., 2018a; Zayed et al., 2017).

The steep portions (1st stage) denote that exterior mass transfer and /or boundary diffusion layer could be the inspiring step of MO ions adsorption by AC binding sites (Naiya et al., 2009; Wang and Zhu, 2006). Such portion (1st stage) is missing in MB plot as a sign of rapid accomplishment of the external surface adsorption (Suganya and Senthil Kumar, 2018). The quiet-slope portions (2nd stage) for the regarded dyes, point to steady ions sorption by  $AC_{(2:1)}$ ; IDP was the main mechanism (Agarwal et al., 2016). So, the 2nd stage was used to estimate the C and  $K_p$  constants (Chen et al., 2010) as depicted in Table 7. The plateau portions (3rd stage) reflect the attained equilibrium state with almost fixed rate of ions sorption by the regarded AC.

As well, the high C values (69.875 and 108.3 mg/g for MB & MO, orderly) validated that their ions removal by  $AC_{(2:1)}$  was not totally defined by IPD, but several diffusion types may be incorporated (Abdulhameed et al., 2019; Gusain et al., 2016; Selim et al., 2018a; Zayed et al., 2017). Such constant values reflect the effective participation of the AC surface in MO removal better than in MB.

#### 4. Conclusion

The outputs of the current work were compiled in the following points:

- The environment-polluting LSB wastes accumulated annually after sugar beet crop harvesting, were successfully transformed into sustainable/high market value ACs through a simplified thermochemical activation process.
- The activation process of the produced ACs was improved by applying different ratios of robust activating agents (0.5:1, 1:1, 2:1, and 3:1 of  $H_3PO_4$ /LSB) that served as a pyrolytic decomposer of the LSB during the calcination process ( $550\text{ }^\circ\text{C}/2\text{h}$ ), impeding the ash formation.
- The highest degree of amorphicity and  $S_{BET}$  ( $700.7\text{ m}^2/\text{g}$ ) nominated  $AC_{(2:1)}$  for MO and MB remediation from synthetic solutions.
- The sorption process MO & MB by the prepared  $AC_{(2:1)}$  was a pH-and time-reliant procedure; the maximum removal capacity was attained at pH 3.0 & 9.0 and equilibrium was reached at 60, and 15 min, orderly.
- The kinetics of MO and MB sorption process by the  $AC_{(2:1)}$ , were illustrated-well by the PSO model following the attained high  $R^2 = 1$  and the approximate agreement among the experimental and theoretical  $q_e$  values.
- The IDP was not the only inspiring step in the sorption process of MO and MB dyes by the prepared  $AC_{(2:1)}$ , but other diffusion styles may be incorporated.
- The isotherm study revealed that the sorption procedure of the investigated dyes was explained well by Langmuir equation, confirming the separate accumulation of each of these contaminant's ions as a homogeneous monolayer upon the surface of the addressed activated carbon via isoenergetic N-and O-bearing binding sites.
- Finally, the synthesized  $AC_{(2:1)}$  is categorized as a superior/ eco-friendly adsorbent for both thiazine and azo dyes with some privilege for the former.

#### Acknowledgment

The work is supported by Science, Technology & Innovation Funding Authority (STDF), Targeted Call Supporting Textile Industry under grant number 43472, Egypt.

## References

- Abdi, J., Mahmoodi, N.M., Vossoughi, M., Alemzadeh, I., 2019. Synthesis of magnetic metal-organic framework nanocomposite ( $ZIF-8@SiO_2@MnFe_2O_4$ ) as a novel adsorbent for selective dye removal from multicomponent systems. *Microporous Mesoporous Mater.* 273, 177–188.
- Abdulhameed, A.S., Mohammad, A.-T., Jawad, A.H., 2019. Application of response surface methodology for enhanced synthesis of chitosan tripolyphosphate/TiO<sub>2</sub> nanocomposite and adsorption of reactive orange 16 dye. *J. Clean. Prod.* 232, 43–56.
- Adinata, D., Wan Daud, W.M.A., Aroua, M.K., 2007. Preparation and characterization of activated carbon from palm shell by chemical activation with K<sub>2</sub>CO<sub>3</sub>. *Bioresour. Technol.* 98, 145–149.
- Agarwal, S., Tyagi, I., Gupta, V.K., Ghasemi, N., Shahivand, M., Ghasemi, M., 2016. Kinetics, equilibrium studies and thermodynamics of methylene blue adsorption on *Ephedra strobilacea* saw dust and modified using phosphoric acid and zinc chloride. *J. Mol. Liq.* 218, 208–218.
- Ahmad, A., Hameed, B., 2010. Effect of preparation conditions of activated carbon from bamboo waste for real textile wastewater. *J. Hazard. Mater.* 173, 487–493.
- Akhair, S.H.M., Harun, Z., Basri, H., Ahmad, R.A.R., Rashid, A.Q. A., Azhar, F.H., 2018. Hydrophobicity properties of graphite and reduced graphene oxide of the Polysulfone (PSf) mixed matrix membrane. *Int. J. Eng.* 31, 1381–1388.
- Albatrni, H., Qiblawey, H., Al-Marri, M.J., 2022. Walnut shell based adsorbents: A review study on preparation, mechanism, and application. *J. Water Process Eng.* 45, 102527.
- Al-Qodah, Z., Shawabkah, R., 2009. Production and characterization of granular activated carbon from activated sludge. *Braz. J. Chem. Eng.* 26, 127–136.
- Altundogan, H.S., Bahar, N., Mujde, B., Tumen, F., 2007. The use of sulphuric acid-carbonization products of sugar beet pulp in Cr(VI) removal. *J. Hazard. Mater.* 144, 255–264.
- Aluigi, A., Tonetti, C., Vineis, C., Tonin, C., Mazzuchetti, G., 2011. Adsorption of copper(II) ions by keratin/PA6 blend nanofibres. *Eur. Polym. J.* 47, 1756–1764.
- Anisuzzaman, S.M., Joseph, C.G., Daud, W.M.A.B.W., Krishnaiyah, D., Yee, H.S., 2015. Preparation and characterization of activated carbon from *Typha orientalis* leaves. *Int. J. Ind. Chem.* 6, 9–21.
- Arumugam, M., Seralathan, K.-K., Praserthdam, S., Tahir, M., Praserthdam, P., 2022. Synthesis of novel graphene aerogel encapsulated bismuth oxyiodide composite towards effective removal of methyl orange azo-dye under visible light. *Chemosphere* 303, 135121.
- Asuha, S., Zhou, X.G., Zhao, S., 2010. Adsorption of methyl orange and Cr(VI) on mesoporous TiO<sub>2</sub> prepared by hydrothermal method. *J. Hazard. Mater.* 181, 204–210.
- Ayad, M.M., El-Nasr, A.A., 2010. Adsorption of Cationic Dye (Methylene Blue) from water using polyaniline nanotubes base. *J. Phys. Chem. C* 114, 14377–14383.
- Azargohar, R., Dalai, A.K., 2006. Biochar As a Precursor of Activated Carbon. In: McMillan, J.D., Adney, W.S., Mielenz, J. R., Klasson, K.T. (Eds.), Twenty-Seventh Symposium on Biotechnology for Fuels and Chemicals. Humana Press, Totowa, NJ, pp. 762–773.
- Barrett, E.P., Joyner, L.G., Halenda, P.P., 1951. The determination of pore volume and area distributions in porous substances. I. Computations from nitrogen isotherms. *J. Am. Chem. Soc.* 73, 373–380.
- Baseri, J.R., Palanisamy, P.N., Sivakumar, P., 2012. Preparation and characterization of activated carbon from *Thevetia peruviana* for the removal of dyes from textile waste water. *Adv. Appl. Sci. Res.* 3, 377–383.
- Bayomie, O.S., Kandeel, H., Shoeib, T., Yang, H., Youssef, N., El-Sayed, M.M.H., 2020. Novel approach for effective removal of methylene blue dye from water using fava bean peel waste. *Sci. Rep.* 10, 7824.
- Brunauer, S., Emmett, P.H., Teller, E., 1938. Adsorption of gases in multimolecular layers. *J. Am. Chem. Soc.* 60, 309–319.
- Budinova, T., Ekinci, E., Yardim, F., Grimm, A., Björnbom, E., Minkova, V., Goranova, M., 2006. Characterization and application of activated carbon produced by H<sub>3</sub>PO<sub>4</sub> and water vapor activation. *Fuel Process. Technol.* 87, 899–905.
- Burgess-Clifford, C.E., Narayanan, D.L., Van Essendelft, D.T., Jain, P., Sakti, A., Lueking, A.D., 2009. The effect of calcination on reactive milling of anthracite as potential precursor for graphite production. *Fuel Process. Technol.* 90, 1515–1523.
- Canales-Flores, R.A., Prieto-García, F., 2020. Taguchi optimization for production of activated carbon from phosphoric acid impregnated agricultural waste by microwave heating for the removal of methylene blue. *Diamond Relat. Mater.* 109, 108027.
- Chatir, E.M., El Hadrami, A., Ojala, S., Brahmi, R., 2022. Production of activated carbon with tunable porosity and surface chemistry via chemical activation of hydrochar with phosphoric acid under oxidizing atmosphere. *Surf. Interfaces* 30, 101849.
- Chaúque, E.F.C., Dlamini, L.N., Adelodun, A.A., Greylung, C.J., Ngila, J.C., 2017. Electrospun polyacrylonitrile nanofibers functionalized with EDTA for adsorption of ionic dyes. *Phys. Chem. Earth, Parts A/B/C* 100, 201–211.
- Cheah, W., Hosseini, S., Khan, M.A., Chuah, T.G., Choong, T.S.Y., 2013. Acid modified carbon coated monolith for methyl orange adsorption. *Chem. Eng. J.* 215–216, 747–754.
- Chen, S., Zhang, J., Zhang, C., Yue, Q., Li, Y., Li, C., 2010. Equilibrium and kinetic studies of methyl orange and methyl violet adsorption on activated carbon derived from *Phragmites australis*. *Desalination* 252, 149–156.
- Corcho-Corral, B., Olivares-Marín, M., Fernández-González, C., Gómez-Serrano, V., Macías-García, A., 2006. Preparation and textural characterisation of activated carbon from vine shoots (*Vitis vinifera*) by H<sub>3</sub>PO<sub>4</sub>—chemical activation. *Appl. Surf. Sci.* 252, 5961–5966.
- Cruz, G., Pirilä, M., Huuhtanen, M., Carrión, L., Alvarenga, E., Keiski, R.L., 2012. Production of activated carbon from cocoa (*Theobroma cacao*) pod husk. *J. Civ. Environ. Eng.* 2, 1–6.
- Cunha, M.R., Lima, E.C., Lima, D.R., da Silva, R.S., Thue, P.S., Seliem, M.K., Sher, F., dos Reis, G.S., Larsson, S.H., 2020. Removal of captorpril pharmaceutical from synthetic pharmaceutical-industry wastewaters: Use of activated carbon derived from *Butia catarinensis*. *J. Environ. Chem. Eng.* 8, 104506.
- Danish, M., Hashim, R., Ibrahim, M.N.M., Rafatullah, M., Ahmad, T., Sulaiman, O., 2011. Characterization of *Acacia mangium* wood based activated carbons prepared in the presence of basic activating agents. *BioResources* 6, 3019–3033.
- Danish, M., Hashim, R., Ibrahim, M., Sulaiman, O., 2014a. Optimization study for preparation of activated carbon from *Acacia mangium* wood using phosphoric acid. *Wood Sci. Technol.* 48, 1069–1083.
- Danish, M., Hashim, R., Ibrahim, M.M., Sulaiman, O., 2014b. Optimized preparation for large surface area activated carbon from date (*Phoenix dactylifera* L.) stone biomass. *Biomass Bioenergy* 61, 167–178.
- Danish, M., Pin, Z., Ziyang, L., Ahmad, T., Majeed, S., Ahmad Yahya, A.N., Khanday, W.A., Abdul Khalil, H.P.S., 2022. Preparation and characterization of banana trunk activated carbon using H<sub>3</sub>PO<sub>4</sub> activation: a rotatable central composite design approach. *Mater. Chem. Phys.* 282, 125989.
- Demiral, H., Demiral, İ., Tümsek, F., Karabacakoglu, B., 2008. Pore structure of activated carbon prepared from hazelnut bagasse by chemical activation. *Surf. Interface Anal.* 40, 616–619.

- Dias, J.M., Alvim-Ferraz, M.C.M., Almeida, M.F., Rivera-Utrilla, J., Sánchez-Polo, M., 2007. Waste materials for activated carbon preparation and its use in aqueous-phase treatment: A review. *J. Environ. Manage.* 85, 833–846.
- Do, M.H., Phan, N.H., Nguyen, T.D., Pham, T.T.S., Nguyen, V.K., Vu, T.T.T., Nguyen, T.K.P., 2011. Activated carbon/Fe<sub>3</sub>O<sub>4</sub> nanoparticle composite: Fabrication, methyl orange removal and regeneration by hydrogen peroxide. *Chemosphere* 85, 1269–1276.
- Ebadí, A., Rafati, A.A., 2015. Preparation of silica mesoporous nanoparticles functionalized with β-cyclodextrin and its application for methylene blue removal. *J. Mol. Liq.* 209, 239–245.
- Eftekhari-Sis, B., Rahimkhoei, V., Akbari, A., Araghi, H.Y., 2018. Cubic polyhedral oligomeric silsesquioxane nano-cross-linked hybrid hydrogels: synthesis, characterization, swelling and dye adsorption properties. *React. Funct. Polym.* 128, 47–57.
- Ekpete, O.A., Horsfall, M.J.N.R., 2011. Preparation and characterization of activated carbon derived from fluted pumpkin stem waste (*Telfairia occidentalis* Hook F). *Res. J. Chem. Sci.* 1, 10–17.
- El Qada, E.N., Allen, S.J., Walker, G.M., 2008. Influence of preparation conditions on the characteristics of activated carbons produced in laboratory and pilot scale systems. *Chem. Eng. J.* 142, 1–13.
- El-Sheikh, M.N., Metwally, B.S., Mubarak, M.F., Ahmed, H.A., Abdel Moghny, T., Zayed, A.M., 2022a. Fabrication of electro-spun polyamide-weathered basalt nano-composite as a non-conventional membrane for basic and acid dye removal. *Polym. Bull.*, 1–23.
- El-Sheikh, M.N., Metwally, B.S., Mubarak, M.F., Ahmed, H.A., Abdel Moghny, T., Zayed, A.M., 2022b. Fabrication of electro-spun polyamide-weathered basalt nano-composite as a non-conventional membrane for basic and acid dye removal. *Polym. Bull.*
- Fernández, M.V., Jagus, R.J., Agüero, M.V., 2017. Evaluation and characterization of nutritional, microbiological and sensory properties of beet greens. *Acta Sci. Nutr. Health* 1, 37–45.
- Ferreira, L.M., de Melo, R.R., Pimenta, A.S., de Azevedo, T.K.B., de Souza, C.B., 2022. Adsorption performance of activated charcoal from castor seed cake prepared by chemical activation with phosphoric acid. *Biomass Convers. Biorefin.* 12, 1181–1192.
- Freundlich, H., 1906. Over the adsorption in solution. *J. Phys. Chem.* 57, 1100–1107.
- Fu, Q., Lou, J., Zhang, R., Peng, L., Zhou, S., Yan, W., Mo, C., Luo, J., 2021. Highly effective and fast removal of Congo red from wastewater with metal-organic framework Fe-MIL-88NH<sub>2</sub>. *J. Solid State Chem.* 294, 121836.
- Gayathiri, M., Pulingam, T., Lee, K.T., Sudesh, K., 2022. Activated carbon from biomass waste precursors: Factors affecting production and adsorption mechanism. *Chemosphere* 294, 133764.
- Ghorbani, F., Kamari, S., Zamani, S., Akbari, S., Salehi, M., 2020. Optimization and modeling of aqueous Cr(VI) adsorption onto activated carbon prepared from sugar beet bagasse agricultural waste by application of response surface methodology. *Surf. Interfaces* 18, 100444.
- Goswami, R., Dey, A.K., 2022. Use of anionic surfactant-modified activated carbon for efficient adsorptive removal of crystal violet dye. *Adsorpt. Sci. Technol.* 2022, 2357242.
- Gratuito, M., Panyathanmaporn, T., Chumnanklang, R.-A., Sirintuntawittaya, N., Dutta, A., 2008. Production of activated carbon from coconut shell: optimization using response surface methodology. *Bioresour. Technol.* 99, 4887–4895.
- Guo, S., Peng, J., Li, W., Yang, K., Zhang, L., Zhang, S., Xia, H., 2009. Effects of CO<sub>2</sub> activation on porous structures of coconut shell-based activated carbons. *Appl. Surf. Sci.* 255, 8443–8449.
- Guo, D., Qi, G., Chen, D., Niu, J., Liu, Y., Jiao, W., 2023. Removal of nitric oxide from simulated flue gas using aqueous persulfate with activation of ferrous ethylenediaminetetraacetate in the rotating packed bed. *Front. Chem. Sci. Eng.*
- Guo, Y., Rockstraw, D.A., 2007. Activated carbons prepared from rice hull by one-step phosphoric acid activation. *Microporous Mesoporous Mater.* 100, 12–19.
- Gupta, V.K., Suhas, 2009. Application of low-cost adsorbents for dye removal – A review. *J. Environ. Manage.* 90, 2313–2342.
- Gusain, D., Srivastava, V., Sillanpää, M., Sharma, Y.C., 2016. Kinetics and isotherm study on adsorption of chromium on nano crystalline iron oxide/hydroxide: linear and nonlinear analysis of isotherm and kinetic parameters. *Res. Chem. Intermed.* 42, 7133–7151.
- Habiba, U., Siddique, T.A., Li Lee, J.J., Joo, T.C., Ang, B.C., Afifi, A.M., 2018. Adsorption study of methyl orange by chitosan/polyvinyl alcohol/zeolite electrospun composite nanofibrous membrane. *Carbohyd. Polym.* 191, 79–85.
- Hameed, B.H., 2009. Spent tea leaves: A new non-conventional and low-cost adsorbent for removal of basic dye from aqueous solutions. *J. Hazard. Mater.* 161, 753–759.
- Han, Q., Wang, J., Goodman, B.A., Xie, J., Liu, Z., 2020. High adsorption of methylene blue by activated carbon prepared from phosphoric acid treated eucalyptus residue. *Powder Technol.* 366, 239–248.
- Haque, M.M., Haque, M.A., Mosharaf, M.K., Marcus, P.K., 2021. Decolorization, degradation and detoxification of carcinogenic sulfonated azo dye methyl orange by newly developed biofilm consortia. *Saudi J. Biol. Sci.* 28, 793–804.
- Hasanzadeh, V., Rahmanian, O., Heidari, M., 2020. Cefixime adsorption onto activated carbon prepared by dry thermochemical activation of date fruit residues. *Microchim. J.* 152, 104261.
- Heidarinejad, Z., Dehghani, M.H., Heidari, M., Javedan, G., Ali, I., Sillanpää, M., 2020. Methods for preparation and activation of activated carbon: a review. *Environ. Chem. Lett.* 18, 393–415.
- Ho, Y.S., Malarvizhi, R., Sulochana, N., 2009. Equilibrium isotherm studies of methylene blue adsorption onto activated carbon prepared from *Delonix regia* pods. *J. Environ. Prot. Sci.* 3, 111–116.
- Ho, Y.S., McKay, G., 1999. Pseudo-second order model for sorption processes. *Process Biochem.* 34, 451–465.
- Hoang, A.T., Kumar, S., Lichtfouse, E., Cheng, C.K., Varma, R.S., Senthilkumar, N., Phong Nguyen, P.Q., Nguyen, X.P., 2022. Remediation of heavy metal polluted waters using activated carbon from lignocellulosic biomass: an update of recent trends. *Chemosphere* 302, 134825.
- Husien, S., El-tawee, R.M., Salim, A.I., Fahim, I.S., Said, L.A., Radwan, A.G., 2022. Review of activated carbon adsorbent material for textile dyes removal: preparation, and modelling. *Curr. Res. Green Sustain. Chem.* 5, 100325.
- Idris, S., Iyaka, Y.A., Dauda, B.E.N., Ndamitso, M.M., Umar, M.T., 2012. Kinetic study of utilizing groundnut shell as an adsorbent in removing chromium and nickel from dye effluent. *Am. Chem. Sci. J.* 2, 12–24.
- Ioannidou, O., Zabaniotou, A., 2007. Agricultural residues as precursors for activated carbon production—a review. *Renew. Sustain. Energy Rev.* 11, 1966–2005.
- Jasri, K., Abdulhameed, A.S., Jawad, A.H., Alothman, Z.A., Yousef, T.A., Al Duaij, O.K., 2023. Mesoporous activated carbon produced from mixed wastes of oil palm frond and palm kernel shell using microwave radiation-assisted K<sub>2</sub>CO<sub>3</sub> activation for methylene blue dye removal: optimization by response surface methodology. *Diamond Relat. Mater.* 131, 109581.
- Jawad, A.H., Ismail, K., Ishak, M.A.M., Wilson, L.D., 2019a. Conversion of Malaysian low-rank coal to mesoporous activated carbon: structure characterization and adsorption properties. *Chin. J. Chem. Eng.* 27, 1716–1727.
- Jawad, A.H., Mamat, N.F.H., Hameed, B.H., Ismail, K., 2019b. Biofilm of cross-linked Chitosan-Ethylene Glycol Diglycidyl Ether for removal of Reactive Red 120 and Methyl Orange: Adsorption and mechanism studies. *J. Environ. Chem. Eng.* 7, 102965.

- Jawad, A.H., Norrahma, S.S.A., Hameed, B.H., Ismail, K., 2019c. Chitosan-glyoxal film as a superior adsorbent for two structurally different reactive and acid dyes: adsorption and mechanism study. *Int. J. Biol. Macromol.* 135, 569–581.
- Jiang, R., Fu, Y.-Q., Zhu, H.-Y., Yao, J., Xiao, L., 2012. Removal of Methyl Orange from Aqueous Solutions by Magnetic Maghemite/Chitosan Nanocomposite Films: Adsorption Kinetics and Equilibrium. *J. Appl. Polym. Sci.* 125, 540–549.
- Jin, X., Yu, Z., Wu, Y., 2010. Preparation of activated carbon from lignin obtained by straw pulping by KOH and  $K_2CO_3$  chemical activation. *Cellul. Chem. Technol.* 7, 79–85.
- Joseph, C.G., Zain, H.F.M., Dek, S.F., 2006. Treatment of landfill leachate in Kayu Madang, Sabah: textural and physical characterization (part 1). *Malays J. Anal. Sci.* 10, 1–6.
- Kalderis, D., Bethanis, S., Paraskeva, P., Diamadopoulos, E., 2008. Production of activated carbon from bagasse and rice husk by a single-stage chemical activation method at low retention times. *Bioresour. Technol.* 99, 6809–6816.
- Karapınar, H.S., 2022. Adsorption performance of activated carbon synthesis by  $ZnCl_2$ , KOH,  $H_3PO_4$  with different activation temperatures from mixed fruit seeds. *Environ. Technol.* 43, 1417–1435.
- Karić, N., Maia, A.S., Teodorović, A., Atanasova, N., Langergraber, G., Crini, G., Ribeiro, A.R.L., Đolić, M., 2022. Bio-waste valorisation: Agricultural wastes as biosorbents for removal of (in)organic pollutants in wastewater treatment. *Chem. Eng. J. Adv.* 9, 100239.
- Kato, T., Kozai, N., Tanaka, K., Kaplan, D.I., Utsunomiya, S., Ohnuki, T., 2022. Chemical species of iodine during sorption by activated carbon -Effects of original chemical species and fulvic acids. *J. Nucl. Sci. Technol.* 59, 580–589.
- Ketcha, J.M., Dina, D.J.D., Ngomo, H.M., Ndi, N.J., 2012. Preparation and characterization of activated carbons obtained from maize cobs by zinc chloride activation. *Am. Chem. Sci. J.* 2, 136–160.
- Khan, I., Saeed, K., Zekker, I., Zhang, B., Hendi, A.H., Ahmad, A., Ahmad, S., Zada, N., Ahmad, H., Shah, L.A., 2022. Review on methylene blue: its properties, uses, toxicity and photodegradation. *Water* 14, 242.
- Khanday, W.A., Asif, M., Hameed, B.H., 2017. Cross-linked beads of activated oil palm ash zeolite/chitosan composite as a bio-adsorbent for the removal of methylene blue and acid blue 29 dyes. *Int. J. Biol. Macromol.* 95, 895–902.
- Kielbasa, K., Bayar, S., Varol, E.A., Sreńcek-Nazzal, J., Bosacka, M., Miądlicki, P., Serafin, J., Wróbel, R.J., Michalkiewicz, B., 2022. Carbon dioxide adsorption over activated carbons produced from molasses using  $H_2SO_4$ ,  $H_3PO_4$ , HCl, NaOH, and KOH as activating agents. *Molecules* 27, 7467.
- Kilpimaa, S., Runtu, H., Kangas, T., Lassi, U., Kuokkanen, T., 2015. Physical activation of carbon residue from biomass gasification: Novel sorbent for the removal of phosphates and nitrates from aqueous solution. *J. Ind. Eng. Chem.* 21, 1354–1364.
- Kim, C., Zhang, Z., Wang, L., Sun, T., Hu, X., 2016. Core-shell magnetic manganese dioxide nanocomposites modified with citric acid for enhanced adsorption of basic dyes. *J. Taiwan Inst. Chem. Eng.* 67, 418–425.
- Koyuncu, F., Avşar Teymur, Y., Güzel, F., 2022. Application of an industrial agricultural waste-based activated carbon in the treatment of water contaminated with Reactive Blue 19 dye: optimization, kinetic, equilibrium and recyclability analyses. *J. Dispers. Sci. Technol.*, 1–12.
- Kumar Biswal, A., Sahoo, M., Kumar Suna, P., Panda, L., Lenka, C., Kumari Misra, P., 2022. Exploring the adsorption efficiency of a novel cellulosic material for removal of food dye from water. *J. Mol. Liq.* 350, 118577.
- Kumar, A., Jena, H.M., 2016. Preparation and characterization of high surface area activated carbon from Fox nut (*Euryale ferox*) shell by chemical activation with  $H_3PO_4$ . *Results Phys.* 6, 651–658.
- Lafi, R., Hafiane, A., 2016. Removal of methyl orange (MO) from aqueous solution using cationic surfactants modified coffee waste (MCWs). *J. Taiwan Inst. Chem. Eng.* 58, 424–433.
- Langmuir, I., 1916. The constitution and fundamental properties of solids and liquids. Part I Solids. *J. Am. Chem. Soc.* 38, 2221–2295.
- Leodopoulos, D., Doulia, D., Gimouhopoulos, K., Triantis, T.M., 2012. Single and simultaneous adsorption of methyl orange and humic acid onto bentonite. *Appl. Clay Sci.* 70, 84–90.
- León, M., Silva, J., Carrasco, S., Barrientos, N., 2020. Design, cost estimation and sensitivity analysis for a production process of activated carbon from waste nutshells by physical activation. *Processes* 8, 945.
- Lewoyehu, M., 2021. Comprehensive review on synthesis and application of activated carbon from agricultural residues for the remediation of venomous pollutants in wastewater. *J. Anal. Appl. Pyrol.* 159, 105279.
- Li, K., Zheng, Z., Li, Y., 2010. Characterization and lead adsorption properties of activated carbons prepared from cotton stalk by one-step  $H_3PO_4$  activation. *J. Hazard. Mater.* 181, 440–447.
- Liou, T.-H., 2010. Development of mesoporous structure and high adsorption capacity of biomass-based activated carbon by phosphoric acid and zinc chloride activation. *Chem. Eng. J.* 158, 129–142.
- Liu, X.-J., Li, M.-F., Singh, S.K., 2021. Manganese-modified lignin biochar as adsorbent for removal of methylene blue. *J. Mater. Res. Technol.* 12, 1434–1445.
- Luo, X., Zheng, H., Lai, W., Yuan, P., Li, S., Li, D., Chen, Y., 2022. Defect engineering of carbons for energy conversion and storage applications. *Energy Environ. Mater.*
- Ma, J., Yu, F., Zhou, L., Jin, L., Yang, M., Luan, J., Tang, Y., Fan, H., Yuan, Z., Chen, J., 2012. Enhanced adsorptive removal of methyl orange and methylene blue from aqueous solution by alkali-activated multiwalled carbon nanotubes. *ACS Appl. Mater. Interfaces* 4 (11), 5749–5760.
- Malekbala, M.R., Hosseini, S., Kazemi Yazdi, S., Masoudi Soltani, S., Malekbala, M.R., 2012. The study of the potential capability of sugar beet pulp on the removal efficiency of two cationic dyes. *Chem. Eng. Res. Des.* 90, 704–712.
- Manoochehri, M., Khorsand, A., Hashemi, E., 2012. Role of modified activated carbon by  $H_3PO_4$  or  $K_2CO_3$  from natural adsorbent for removal of Pb (II) from aqueous solutions. *Carbon Lett.* 13, 115–120.
- Marandi, A., Kolvari, E., Gilandoust, M., Zolfogol, M.A., 2022. Immobilization of  $-OSO_3H$  on activated carbon powder and its use as a heterogeneous catalyst in the synthesis of phthalazine and quinoline derivatives. *Diamond Relat. Mater.* 124, 108908.
- Massaro, M., Colletti, C.G., Lazzara, G., Guernelli, S., Noto, R., Riela, S., 2017. Synthesis and Characterization of Halloysite-Cyclodextrin Nanosplices for Enhanced Dyes Adsorption. *ACS Sustain. Chem. Eng.* 5 (4), 3346–3352.
- Md Zaini, M.S., Anuar, N.F., Al-Junid, S.A.M., Syed-Hassan, S.S. A., 2023. Agricultural biomass-based carbon cathode materials for lithium-sulfur batteries: a systematic review. *Mater. Sci. Energy Technol.* 6, 205–225.
- Merzougui, Z., Addoun, F., 2008. Effect of oxidant treatment of date pit activated carbons application to the treatment of waters. *Desalination* 222, 394–403.
- Mohamed, F.M., Li, Z., Zayed, A.M., 2020. Carbon nanotube impregnated anthracite (An/CNT) as a superior sorbent for azo dye removal. *RSC Adv.* 10, 25586–25601.
- Mohamed, E.A., Selim, A.Q., Zayed, A.M., Komarneni, S., Mobarak, M., Seliem, M.K., 2019. Enhancing adsorption capacity of Egyptian diatomaceous earth by thermo-chemical purification: Methylene blue uptake. *J. Colloid Interface Sci.* 534, 408–419.
- Mohammadi, N., Khani, H., Gupta, V.K., Amereh, E., Agarwal, S., 2011. Adsorption process of methyl orange dye onto mesoporous carbon material—kinetic and thermodynamic studies. *J. Colloid Interface Sci.* 362, 457–462.

- Mokhtari, P., Ghaedi, M., Dashtian, K., Rahimi, M.R., Purkait, M.K., 2016. Removal of methyl orange by copper sulfide nanoparticles loaded activated carbon: Kinetic and isotherm investigation. *J. Mol. Liq.* 219, 299–305.
- Mubarak, M.F., Zayed, A.M., Ahmed, H.A., 2022. Activated Carbon/Carborundum@Microcrystalline Cellulose core shell nano-composite: Synthesis, characterization and application for heavy metals adsorption from aqueous solutions. *Ind. Crop. Prod.* 182, 114896.
- Naiya, T.K., Bhattacharya, A.K., Mandal, S., Das, S.K., 2009. The sorption of lead(II) ions on rice husk ash. *J. Hazard. Mater.* 163, 1254–1264.
- Natrayan, L., Arul Kumar, P.V., Dhanraj, J.A., Kaliappan, S., Sivakumar, N.S., Patil, P.P., Sekar, S., Paramasivam, P., 2022. Synthesis and analysis of impregnation on activated carbon in multiwalled carbon nanotube for Cu adsorption from wastewater. *Bioinorg. Chem. Appl.* 2022, 7470263.
- Nazem, M.A., Zare, M.H., Shirazian, S., 2020. Preparation and optimization of activated nano-carbon production using physical activation by water steam from agricultural wastes. *RSC Adv.* 10, 1463–1475.
- Nazir, M.A., Khan, N.A., Cheng, C., Shah, S.S.A., Najam, T., Arshad, M., Sharif, A., Akhtar, S., Rehman, A.U., 2020. Surface induced growth of ZIF-67 at Co-layered double hydroxide: removal of methylene blue and methyl orange from water. *Appl. Clay Sci.* 190, 105564.
- Neme, I., Gonfa, G., Masi, C., 2022. Activated carbon from biomass precursors using phosphoric acid: a review. *Heliyon* 8, e11940.
- Ngofa, O.N., Liakos, E.V., Papadopoulos, A.N., Kyzas, G.Z., 2022. Activated carbon from bamboo and banana wood fibers as adsorbent materials for the removal of oil samples. *Biointerface Res. Appl. Chem.* 12, 2701–2714.
- Ninfali, P., Angelino, D., 2013. Nutritional and functional potential of Beta vulgaris cicla and rubra. *Fitoterapia* 89, 188–199.
- Norouzi, S., Heidari, M., Alipour, V., Rahamanian, O., Fazlzadeh, M., Mohammadi-moghadam, F., Nourmoradi, H., Goudarzi, B., Dindarloo, K., 2018. Preparation, characterization and Cr(VI) adsorption evaluation of NaOHactivated carbon produced from Date Press Cake; an agro-industrial waste. *Bioresour. Technol.* 258, 48–56.
- Omri, A., Benzina, M., 2012. Characterization of activated carbon prepared from a new raw lignocellulosic material: *Ziziphus spina-christi* seeds. *Journal de la Société Chimique de Tunisie* 14, 175–183.
- Önal, Y., Akmil-Başar, C., Sarıcı-Özdemir, Ç., Erdoğan, S., 2007. Textural development of sugar beet bagasse activated with ZnCl<sub>2</sub>. *J. Hazard. Mater.* 142, 138–143.
- Örkün, Y., Karatepe, N., Yavuz, R., 2012. Influence of temperature and impregnation ratio of H<sub>3</sub>PO<sub>4</sub> on the production of activated carbon from hazelnut shell. *Acta Physica Polonica-Series A General Physics* 121, 277.
- Ozpınar, P., Dogan, C., Demiral, H., Morali, U., Erol, S., Samdan, C., Yıldız, D., Demiral, I., 2022. Activated carbons prepared from hazelnut shell waste by phosphoric acid activation for supercapacitor electrode applications and comprehensive electrochemical analysis. *Renew. Energy* 189, 535–548.
- Prahas, D., Kartika, Y., Indraswati, N., Ismadji, S., 2008. Activated carbon from jackfruit peel waste by H<sub>3</sub>PO<sub>4</sub> chemical activation: Pore structure and surface chemistry characterization. *Chem. Eng. J.* 140, 32–42.
- Rafatullah, M., Sulaiman, O., Hashim, R., Ahmad, A., 2010. Adsorption of methylene blue on low-cost adsorbents: a review. *J. Hazard. Mater.* 177, 70–80.
- Sahu, J.N., Acharya, J., Meikap, B.C., 2010. Optimization of production conditions for activated carbons from Tamarind wood by zinc chloride using response surface methodology. *Bioresour. Technol.* 101, 1974–1982.
- Saleh, T.A., Al-Saadi, A.A., Gupta, V.K., 2014. Carbonaceous adsorbent prepared from waste tires: Experimental and computational evaluations of organic dye methyl orange. *J. Mol. Liq.* 191, 85–91.
- Sekirifa, M.L., Hadj-Mahammed, M., Pallier, S., Baameur, L., Richard, D., Al-Dujaili, A.H., 2013. Preparation and characterization of an activated carbon from a date stones variety by physical activation with carbon dioxide. *J Anal Appl Pyrol* 99, 155–160.
- Selim, A.Q., Mohamed, E.A., Mobarak, M., Zayed, A.M., Seliem, M.K., Komarneni, S., 2018a. Cr(VI) uptake by a composite of processed diatomite with MCM-41: Isotherm, kinetic and thermodynamic studies. *Microporous Mesoporous Mater.* 260, 84–92.
- Selim, A.Q., Mohamed, E.A., Seliem, M.K., Zayed, A.M., 2018b. Synthesis of sole cancrinite phase from raw muscovite: Characterization and optimization. *J. Alloys Compd.* 762, 653–667.
- Senthil Kumar, P., Fernando, P.S.A., Ahmed, R.T., Srinath, R., Priyadarshini, M., Vignesh, A., Thanjiappan, A., 2014. Effect of temperature on the adsorption of methylene blue dye onto sulfuric acid-treated orange peel. *Chem. Eng. Commun.* 201, 1526–1547.
- Shahabuddin, S., Sarih, N.M., Mohamad, S., Baharin, S.N.A., 2016. Synthesis and characterization of Co<sub>3</sub>O<sub>4</sub> nanocube-doped polyani-line nanocomposites with enhanced methyl orange adsorption from aqueous solution. *RSC Adv.* 6 (49), 43388–43400.
- Shamsuddin, M.S., Yusoff, N.R.N., Sulaiman, M.A., 2016. Synthesis and characterization of activated carbon produced from kenaf core fiber using H<sub>3</sub>PO<sub>4</sub> activation. *Procedia Chem.* 19, 558–565.
- Shiue, A., Ma, C.-M., Ruan, R.-T., Chang, C.-T., 2012. Adsorption kinetics and isotherms for the removal methyl orange from wastewaters using copper oxide catalyst prepared by the waste printed circuit boards. *Environ. Res.* 22, 209–215.
- Singh, D., Verma, S., Gautam, R.K., Krishna, V., 2015. Copper adsorption onto synthesized nitrilotriacetic acid functionalized Fe<sub>3</sub>O<sub>4</sub> nanoparticles: kinetic, equilibrium and thermodynamic studies. *J. Environ. Chem. Eng.* 3, 2161–2171.
- Sirajo, L., Ahmad Zaini, M.A., 2023. Adsorption of water pollutants using H<sub>3</sub>PO<sub>4</sub>-activated lignocellulosic agricultural waste: a mini review. *Toxin Rev.* 42, 349–361.
- Soleimani, M., Kaghazchi, T., 2007. Agricultural waste conversion to activated carbon by chemical activation with phosphoric acid. *Chem. Eng. Technol.: Ind. Chem.-Plant Equipment-Process Eng.-Biotechnol.* 30, 649–654.
- Sriram, G., Bendre, A., Altalhi, T., Jung, H.-Y., Hegde, G., Kurkuri, M., 2022. Surface engineering of silica based materials with Ni–Fe layered double hydroxide for the efficient removal of methyl orange: Isotherms, kinetics, mechanism and high selectivity studies. *Chemosphere* 287, 131976.
- Su, Y., Jiao, Y., Dou, C., Han, R., 2014. Biosorption of methyl orange from aqueous solutions using cationic surfactant-modified wheat straw in batch mode. *Desalin. Water Treat.* 52, 6145–6155.
- Subbaiah, M.V., Kim, D.-S., 2016. Adsorption of methyl orange from aqueous solution by aminated pumpkin seed powder: Kinetics, isotherms, and thermodynamic studies. *Ecotoxicol. Environ. Saf.* 128, 109–117.
- Subha, R., Namasisavayam, C., 2009. Zinc chloride activated coir pith carbon as low cost adsorbent for removal of 2, 4-dichlorophenol: equilibrium and kinetic studies.
- Suganya, S., Senthil Kumar, P., 2018. Influence of ultrasonic waves on preparation of active carbon from coffee waste for the reclamation of effluents containing Cr(VI) ions. *J. Ind. Eng. Chem.* 60, 418–430.
- Swaminathan, S., Muthumanickam, A., Imayathamizhan, N.M., 2015. An effective removal of methylene blue dye using polyacrylonitrile yarn waste/graphene oxide nanofibrous composite. *Int. J. Environ. Sci. Technol. (Tehran)* 12, 3499–3508.
- Sych, N.V., Trofymenko, S.I., Poddubnaya, O.I., Tsypa, M.M., Sapsay, V.I., Klymchuk, D.O., Puziy, A.M., 2012. Porous structure and surface chemistry of phosphoric acid activated carbon from corncob. *Appl. Surf. Sci.* 261, 75–82.

- Tan, I.A.W., Ahmad, A.L., Hameed, B.H., 2008. Adsorption of basic dye on high-surface-area activated carbon prepared from coconut husk: Equilibrium, kinetic and thermodynamic studies. *J. Hazard. Mater.* 154, 337–346.
- Thommes, M., Kaneko, K., Neimark, A.V., Olivier, J.P., Rodriguez-Reinoso, F., Rouquerol, J., Sing, K.S.W., 2015. Physisorption of gases, with special reference to the evaluation of surface area and pore size distribution. (IUPAC Technical Report) 87, 1051–1069.
- Tiwari, S.K., Bystrzejewski, M., De Adhikari, A., Huczko, A., Wang, N., 2022. Methods for the conversion of biomass waste into value-added carbon nanomaterials: Recent progress and applications. *Prog. Energy Combust. Sci.* 92, 101023.
- Tran, H.N., You, S.-J., Chao, H.-P., 2017a. Fast and efficient adsorption of methylene green 5 on activated carbon prepared from new chemical activation method. *J. Environ. Manage.* 188, 322–336.
- Tran, H.N., You, S.-J., Chao, H.-P., 2017b. Insight into adsorption mechanism of cationic dye onto agricultural residues-derived hydrochars: Negligible role of  $\pi$ - $\pi$  interaction. *Korean J. Chem. Eng.* 34, 1708–1720.
- Tucureanu, V., Matei, A., Avram, A.M., 2016. FTIR spectroscopy for carbon family study. *Crit. Rev. Anal. Chem.* 46, 502–520.
- Tuli, F.J., Hossain, A., Kibria, A.K.M.F., Tareq, A.R.M., Mamun, S.M.M.A., Ullah, A.K.M.A., 2020. Removal of methylene blue from water by low-cost activated carbon prepared from tea waste: A study of adsorption isotherm and kinetics. *Environ. Nanotechnol. Monit. Manage.* 14, 100354.
- Ullah, A., Zahoor, M., Din, W.U., Muhammad, M., Khan, F.A., Sohail, A., Ullah, R., Ali, E.A., Murthy, H.C.A., 2022. Removal of Methylene Blue from Aqueous Solution Using Black Tea Wastes: Used as Efficient Adsorbent. *Adsorpt. Sci. Technol.* 2022, 5713077.
- Umpuch, C., Sakaew, S., 2013. Removal of methyl orange from aqueous solutions by adsorption using chitosan intercalated montmorillonite. *Songklanakarin. J. Sci. Technol.* 35.
- Wang, L., Li, Z., Chen, J., Huang, Y., Zhang, H., Qiu, H., 2019a. Enhanced photocatalytic degradation of methyl orange by porous graphene/ZnO nanocomposite. *Environ. Pollut.* 249, 801–811.
- Wang, Y., Qi, Z., Liu, H., Zhang, J., Peng, L., 2022. Fabrication of zirconium-doped activated carbon by chemical activation for catalytic transfer hydrogenation of 5-Hydroxymethylfurfural into 2,5-Dihydroxymethylfuran. *Energy Fuel* 36, 13796–13807.
- Wang, Q., Wang, Y., Chen, L., 2019b. A green composite hydrogel based on cellulose and clay as efficient absorbent of colored organic effluent. *Carbohydr. Polym.* 210, 314–321.
- Wang, L., Zhang, J., Wang, A., 2011. Fast removal of methylene blue from aqueous solution by adsorption onto chitosan-g-poly (acrylic acid)/attapulgite composite. *Desalination* 266, 33–39.
- Wang, S., Zhu, Z.H., 2006. Characterisation and environmental application of an Australian natural zeolite for basic dye removal from aqueous solution. *J. Hazard. Mater.* 136, 946–952.
- Weber, T.W., Chakravo, R.K., 1974. Pore and Solid Diffusion Models for Fixed-Bed Adsorbers. *AIChE Journal* 20, 228–238.
- Weber, J.C., Morris, W.J., 1962. In: Advances in water pollution research: removal of biologically resistant pollutant from waste water by adsorption, 2. Proceedings of International Conference on Water Pollution Symposium, Pergamon, pp. 231–266.
- Xiong, J., Jiao, C., Li, C., Zhang, D., Lin, H., Chen, Y., 2014. A versatile amphiprotic cotton fiber for the removal of dyes and metal ions. *Cellul.* 21 (4), 3073–3087.
- Xu, J., Chen, L., Qu, H., Jiao, Y., Xie, J., Xing, G., 2014. Preparation and characterization of activated carbon from reedy grass leaves by chemical activation with H<sub>3</sub>PO<sub>4</sub>. *Appl. Surf. Sci.* 320, 674–680.
- Yahya, M.A., Al-Qodah, Z., Ngah, C.Z., 2015. Agricultural bio-waste materials as potential sustainable precursors used for activated carbon production: a review. *Renew. Sustain. Energy Rev.* 46, 218–235.
- Yao, Y., Wang, L., Sun, L., Zhu, S., Huang, Z., Mao, Y., Lu, W., Chen, W., 2013. Efficient removal of dyes using heterogeneous Fenton catalysts based on activated carbon fibers with enhanced activity. *Chem. Eng. Sci.* 101, 424–431.
- Yee, L.F., Abdullah, M.P., Abdullah, A., Ishak, B., Abidin, K.N.Z., 2009. Hydrophobicity characteristics of natural organic matter and the formation of THM. *The Malaysian J. Anal. Sci.* 13, 94–99.
- Yuan, J., Passeport, E., Hofmann, R., 2022. Understanding adsorption and biodegradation in granular activated carbon for drinking water treatment: a critical review. *Water Res.* 210, 118026.
- Zayed, A.M., Selim, A.Q., Mohamed, E.A., Abdel Wahed, M.S.M., Seliem, M.K., Sillanpää, M., 2017. Adsorption characteristics of Na-A zeolites synthesized from Egyptian kaolinite for manganese in aqueous solutions: response surface modeling and optimization. *Appl. Clay Sci.* 140, 17–24.
- Zayed, A.M., Abdel Wahed, M.S.M., Mohamed, E.A., Sillanpää, M., 2018. Insights on the role of organic matters of some Egyptian clays in methyl orange adsorption: isotherm and kinetic studies. *Appl. Clay Sci.* 166, 49–60.
- Zayed, A.M., Fathy, M., Sillanpää, M., Abdel Wahed, M.S.M., 2020. Talc-graphite schist as a natural organo-mineral complex for methylene blue remediation: kinetic and isotherm study. *SN Appl. Sci.* 2, 740.
- Zhang, X.P., Zhang, C., Tan, P., Li, X., Fang, Q.-Y., Chen, G., 2018. Effects of hydrothermal upgrading on the physicochemical structure and gasification characteristics of Zhundong coal. *Fuel Process. Technol.* 172, 200–208.
- Zhang, R., Zhou, Y., Gu, X., Lu, J., 2015. “Competitive Adsorption of Methylene Blue and Cu<sup>2+</sup> onto Citric Acid Modified Pine Sawdust. *CLEAN – Soil, Air Water* 43 (1), 96–103.
- Zhao, R., Wang, Y., Li, X., Sun, B., Jiang, Z., Wang, C., 2015. Water-insoluble sericin/ $\beta$ -cyclodextrin/PVA composite electrospun nanofibers as effective adsorbents towards methylene blue. *Colloids Surf. B Biointerfaces* 136, 375–382.
- Zhengrong, G., Xiaomin, W., 2013. Carbon materials from high ash bio-char: a nanostructure similar to activated grapheme. *Am Trans Eng Appl Sci* 2, 15–34.
- Zhu, X., He, M., Sun, Y., Xu, Z., Wan, Z., Hou, D., Alessi, D.S., Tsang, D.C.W., 2022. Insights into the adsorption of pharmaceuticals and personal care products (PPCPs) on biochar and activated carbon with the aid of machine learning. *J. Hazard. Mater.* 423, 127060.
- Zirak, M., Abdollahiyan, A., Eftekhari-Sis, B., Saraei, M., 2018. Carboxymethyl cellulose coated Fe<sub>3</sub>O<sub>4</sub>@SiO<sub>2</sub> core–shell magnetic nanoparticles for methylene blue removal: equilibrium, kinetic, and thermodynamic studies. *Cellul.* 25 (1), 503–515.